Nano Research
2020, 13(12): 3183–3197

ISSN 1998-0124 CN 11-5974/O4
https://doi.org/10.1007/s12274-020-3031-2

Review Article

Plasmon-generated hot holes for chemical reactions

Chengyu Zhang, Fucan Jia, Zhuoyao Li, Xiao Huang, and Gang Lu (✉)

Key Laboratory of Flexible Electronics (KLOFE) and Institute of Advanced Materials (IAM), Nanjing Tech University (NanjingTech), 30 South Puzhu Road, Nanjing 211816, China

Received: 8 June 2020 / **Revised:** 27 July 2020 / **Accepted:** 4 August 2020

ABSTRACT

Plasmonic nanostructures have been widely used for photochemical conversions due to their unique and easy-tuning optical properties in visible and near-infrared range. Compared with the plasmon-generated hot electrons, the hot holes usually have a shorter lifetime, which makes them more difficult to drive redox reactions. This review focuses on the photochemistry driven by the plasmon-generated hot holes. First, we discuss the generation and energy distribution of the plasmon-generated hot carriers, especially hot holes. Then, the dynamics of the hot holes are discussed at the interface between plasmonic metal and semiconductor or adsorbed molecules. Afterwards, the utilization of these hot holes in redox reactions is reviewed on the plasmon-semiconductor heterostructures as well as on the surface of the molecule-adsorbed plasmonic metals. Finally, the remaining challenges and future perspectives in this field are presented. This review will be helpful for further improving the efficiency of the photochemical reactions involving the plasmon-generated hot holes and expanding the applications of these hot holes in varieties of chemical reactions, especially the ones with high conversion rate and selectivity.

KEYWORDS

surface plasmon, hot hole, photochemistry, photocatalysis

1 Introduction

Solar energy harvesting is one of the most important ways for solving the global problems of energy crisis and environment pollution [1–4]. Photochemical conversion is one of the effective pathways, which could produce not only energy but also chemical compounds that are useful in modern industry [5]. In nature, plants do this at any moment; however, it is still necessary to realize similar process in artificial photosynthesis. Fujishima and Honda first realized the water splitting under solar illumination by using titanium dioxide (TiO_2) as photocatalyst [6]. Since then, many semiconductor-based photocatalysts have been developed for photochemical reactions [7, 8]. However, these semiconductor catalysts are usually limited by the large band gap (only ultraviolet and short wavelength visible light could be utilized) and the poor photo or chemical stability. In order to utilize the visible and near infrared light (which account for majority of the solar energy), it is promising to develop new photocatalysts or strategies for more efficient photosynthesis.

Surface plasmons (SPs), the collective oscillation of free electrons occurred in nanostructures of metals or heavily doped semiconductors, have attracted much attention in the fields of medicine [9], biology [10, 11], and sensing [12, 13]. Due to the surface plasmon resonance, a molecule or nanoparticle in the vicinity of plasmonic metal experiences a much higher absorption coefficient in a large wavelength range, which could in principal introduce a much more efficient photochemical conversion. Moreover, when plasmonic metal forms a heterostructure with a semiconductor, the light absorption could be further broadened due to the synergistic effect between these two materials. For instance, Han and co-workers have reported a broadening of light absorption for roughly two times in a heterostructure of gold and TiO_2 [14]. This broadening in light absorption has also been observed at other heterostructures composed of plasmonic metal and semiconductor materials [15, 16], which could enhance the utilization efficiency of sunlight.

Owing to these optical properties, plasmonic structures could be used in many photochemical reactions, in which a variety of solar energy could be effectively utilized. The excitation of surface plasmon could also introduce three effects: electromagnetic near-field enhancement, charge-carrier excitation, and localized heating, all of which could be useful in photochemical reactions [17, 18]. First, SPs could introduce a localized electromagnetic field in the vicinity of plasmonic nanostructure, which could be orders of magnitude higher than that used for excitation [19]. The enhanced electromagnetic field could mediate or enhance a photochemical reaction, since it increases the excitation probability of the reactant molecules or semiconductor that is close to the plasmonic structure [20], accelerating chemical reactions. For instance, Jang and co-workers have observed three folds of enhancement in water oxidation on the gold nanoparticle-coated bismuth vanadate ($BiVO_4$) crystals [21]. Second, SPs introduce a localized heating, which could trigger a nanoscale chemical reaction. It has been reported that polydimethylsiloxane (PDMS) could be cured locally in the vicinity of plasmonic metal [22]. Except for polymerization, localized heating could also be used for triggering organic transformation of small molecules. Kuwahara and co-workers have reported a plasmonic heating-triggered dehydrogenation of 2,13-bis(aldehyde)[7]thiaheterohelicene molecules at the

Address correspondence to iamglv@njtech.edu.cn

tip of a silver probe [23]. Third, SPs could also introduce the excitation of hot carriers (electrons and holes), which could be injected into the adsorbed molecules or closely contacted semiconductor and drive a redox reaction [24]. The hot carriers, hot electrons and holes, here refer to the carriers with enough energy to drive desired chemical reactions [25]. These three effects usually contribute to the plasmon-mediated chemical reactions simultaneously. It is difficult, sometimes impossible, to distinguish the individual contribution of each effect, even though many attempts have been made in the past few years [26–29].

The plasmon-generated hot electrons and hot holes can both been utilized in redox reactions. For instance, controlled growth of gold has also been achieved on the surface of gold triangular plates due to the accumulation of hot electrons in the adsorbed polyvinylpyrrolidone (PVP) [30]. The generated hot electrons could also drive many other reactions, such as carbon dioxide (CO_2) reduction [31–34] and hydrogen evolution [35–38], at the heterostructures of plasmonic metal and semiconductor. Besides hot electrons, the plasmon-generated hot holes could also be used for driving photochemical reactions, such as water oxidation [39, 40] and metal dissolution [41, 42]. However, compared to the widely studied photochemistry driven by the plasmon-generated hot electrons, the one driven by the hot holes has received much less attention, possibly due to the shorter lifetime of the holes compared with electrons [43, 44].

Since SPs have great advantages in driving chemical reactions, there have been several comprehensive reviews on plasmon-mediated photochemistry [45–48]. In these reviews, the applications of SPs in many chemical reactions have been summarized and the mechanisms of these reactions have also been discussed. Moreover, Huang and co-workers have reviewed the energy and charge transfer in plasmonic photocatalytic composites [49], which is crucial in the plasmon-mediated photochemistry. Wei and co-workers have reviewed the SP-driven hot electron photochemistry, in which the role of plasmon-generated hot electrons in redox reactions has been fully discussed [50]. However, there are still few reviews on the photochemistry driven by the plasmon-generated hot holes. Very recently, Tatsuma and co-workers have reviewed the ejection of hot holes involved in plasmon-induced charge separation [51], which focuses mainly on the behavior of the plasmon-generated hot holes. Note that the contributions of near-filed and plasmonic heating are ignored in this review, since it is difficult, sometimes impossible, to isolate the individual contribution of these plasmonic effects. In this review, the photochemistry involving plasmon-generated hot holes will be discussed in detail. First, we discuss the generation and separation of the hot carriers in plasmonic structure, and then the dynamics of the hot electrons and hot holes, especially the hot holes, at plasmon-semiconductor and plasmon-molecule interfaces. Afterward, the role of the plasmon-generated hot holes in many photochemical reactions is fully discussed. Finally, we present the future perspectives of the plasmon-generated hot holes in various photochemical reactions, especially the ones with high reaction efficiency and selectivity.

2 Generation and transfer of hot holes in plasmonic structures

2.1 Generation and energy distribution of the hot carriers

When a plasmonic nanostructure is illuminated, hot carriers are generated via plasmon decay in the form of non-radiative transition within a time scale of 1 to 100 fs [52]. Afterward, these hot carriers dissipate rapidly via electron-electron and electron-phonon scatterings within 100 fs–1 ps and 1–10 ps, respectively. Finally, their energy is depleted to surrounding medium in the form of heat within a time scale of 100 ps–10 ns (Fig. 1(a)) [46, 53]. As known, the properties of a plasmonic structure are highly dependent on its chemical composition, size, shape, and surrounding media [54–58], which will also affect the hot carrier generation inside. Nordlander and co-workers have designed a model to illustrate the generation of hot carriers in plasmonic metal nanoparticles (Fig. 1(b)) [59]. They found that more hot carriers could be generated in a larger nanoparticle (the one with diameter of 25 nm in Fig. 1(b)) when the lifetime of the carriers is short; however, these carriers are less energetic. Therefore, the generated carriers are not effective in driving photochemical reactions. On the contrary, fewer hot carriers could be generated in a small nanoparticle (the one with diameter of 15 nm in Fig. 1(b)); however, these hot carriers are more effective in driving redox reactions. The efficiency of carrier generation, which refers to the number of hot carriers generated per each plasmon excited in the system, decreases with the increase of energy threshold and particle size and increase with the increase of carrier lifetime [53].

The energy distribution of the plasmon-generated hot carriers is also related to the electronic band structure of the plasmonic metal and the photo energy of the incident light. It is known that the widely used plasmonic metals, such as aluminum, gold, silver, and copper, possess different band structures. The plasmonic peaks of gold and silver usually locate in visible range, while those of aluminum and copper locate in near ultraviolet and visible-near infrared regions, respectively [54–56, 60]. Through theoretical calculation, Atwater and co-workers have illustrated the initial distributions of the hot carriers in these four plasmonic metals [25]. As known, the electrons in plasmonic metal could be excited via the inter-band (d–s) or intra-band (s–s) transition. When inter-band transition dominates, the energy of the generated holes is higher than those of electrons by 1–2 eV in gold and copper, while the generated holes and electrons possess similar energy in aluminum and silver (Fig. 1(c)). Moreover, by using numerical simulation, Louie and co-workers have demonstrated that the energy distribution and mean free path of the hot carriers are highly dependent on the relative positions of the s and d bands in plasmonic metal, and the energy loss and transportation is determined by the electron-phonon interactions (Fig. 1(d)) [61]. If the excitation energy is not high enough for inter-band electronic transition, intra-band transition is the dominated process and the energy of the generated hot electrons and holes is close to each other. In this case, the mean free path of the generated hot carriers is relatively long, which could reach up to 20–40 nm. In contrast, if the excitation energy is high enough for inter-band transition, the generated hot holes are energetic with short mean free path and many of them distribute at the top of d band, while the generated hot electrons are weak in energy. However, if the excitation energy is above 5 eV, the energy is uniformly distributed in the generated hot holes and electrons. The lifetime of holes, which is usually shorter than that of electrons due to the higher group velocities of holes [43], is largely dependent on the choice of material, detailed morphology, energy of the carrier, etc. According to the calculation from Atwater and co-workers, the holes below the Fermi level by < 1.5 eV have lifetime of 10–40 fs [25, 51].

2.2 Hot hole dynamics at heterostructures

The effective separation of the plasmon-generated hot electrons

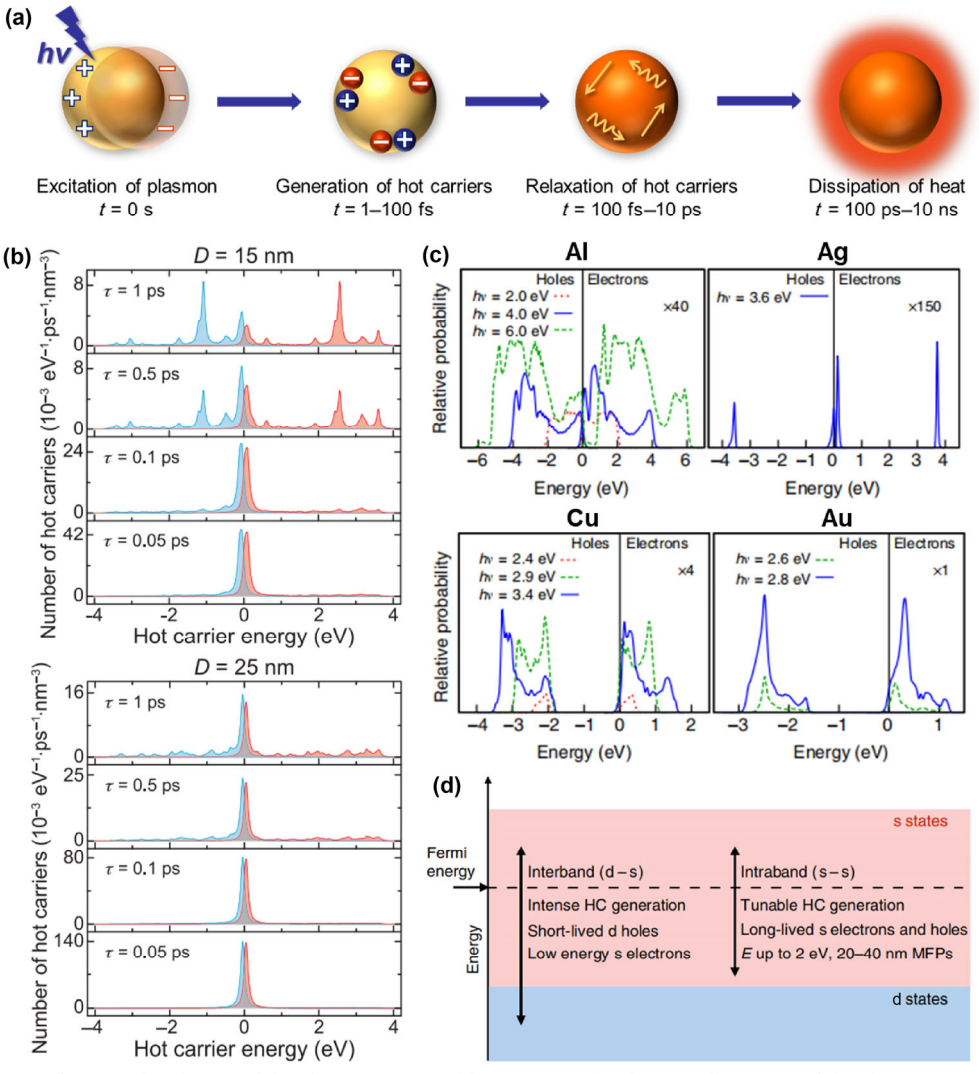

Figure 1 Generation and energy distribution of the plasmon-generated hot carriers. (a) Schematic illustration of the plasmon excitation and relaxation on the surface of a plasmonic metal nanoparticle. The straight yellow arrows represent the electron-electron scattering, while the curved ones represent the electron-phonon scattering. These hot carriers dissipate rapidly within 100 fs–1ps and 1–10 ps, respectively. (b) Energy distributions of the hot electrons (red lines) and hot holes (blue lines) with four different carrier lifetimes (0.05–1 ps) in two nanoparticles with diameters of 15 and 25 nm, respectively. Zero energy refers to the Fermi level. (c) Energy distributions of the hot carriers in aluminum (Al), silver (Ag), copper (Cu) and gold (Au). Zero energy refers to the Fermi level. (d) Hot carriers (HC) generated from plasmon-generated inter-band (d–s) or intra-band (s–s) transition. MFPs refers to the mean free paths, and the dashed line indicates the Fermi energy. Panel (b) is reprinted with permission from Ref. [59], © American Chemical Society 2014. Panel (c) is reprinted with permission from Ref. [62], © Sundararaman, R. et al. 2014. Panel (d) is reprinted with permission from Ref. [61], © Bernardi, M. et al. 2015.

and holes is crucial in driving redox reactions. Effective charge separation could be achieved at the junctions of plasmonic metal with semiconductor or adsorbed molecules. The energy distribution of the generated hot carriers is crucial for separation and utilization of the hot electrons and holes. The hot carriers with higher energy and longer lifetime usually have a higher chance to pass through the barrier at the interface and achieve effective charge separation. In addition, matching the energy level or energy band structure of the adsorbate or semiconductor with the energy distribution of hot carriers is also a key to effective charge separation. With suitable energy band alignment, the excited hot electrons transfer to the adsorbed molecules or the closely contacted semiconductor via the indirect or direct pathway. In indirect pathway, the hot electrons are generated on metal surface via nonradiative decay [43], and these hot electrons could transfer to surrounding media or adsorbed molecules [63]. While in direct pathway, the hot electrons are generated directly in the lowest unoccupied molecular orbital (LUMO) of the adsorbed molecules or conduction band (CB) of the closely contacted semiconductor via another dephasing pathway [64, 65].

2.2.1 *At the plasmon-semiconductor interfaces*

The plasmon-generated hot electrons and holes could be effectively separated at the plasmon-semiconductor interfaces [66, 67]. When forming a junction, the electrons in CB of semiconductor (e.g. n-type) transfer to Fermi level of the metal and an interfacial electric field forms if the work function of the metal is larger than that of semiconductor. As a result, the valence band (VB) and CB in semiconductor bend upwards, and a Schottky barrier forms at the interface [68]. Under this circumstance, the hot electrons from plasmon decay with enough energy can be injected to the CB of semiconductor by passing through the Schottky barrier via indirect or direct transfer pathway, realizing effective separation of hot electrons and holes and prolonging of their lifetime [69]. Therefore, the hot electrons locate inside semiconductor and hot holes remain inside the plasmonic metal, which could be utilized for

reduction and oxidation reactions, respectively (Fig. 2(a)). In contrast, if the work function of the metal is smaller than that of semiconductor (e.g. p-type), the electrons in Fermi level of the metal transfer to CB of the semiconductor. This leads to a downward bending of the CB and VB in the semiconductor close to the interface. A Schottky barrier for holes forms, and the hot holes generated in plasmonic metal with enough energy could transfer to VB of the semiconductor (Fig. 2(b)). Thus, hot holes and hot electrons could be effectively separated and locate in semiconductor and metal, promoting oxidation and reduction reactions, respectively.

Some heavily doped semiconductors have also been proven as effective plasmonic materials in near infrared range [70–72]. When they form heterostructures with other semiconductors, the charge separation process is similar to the case in abovementioned metal-semiconductor heterostructures. For instance, in the heterostructure of cadmium sulfide (CdS) and copper(II) sulfide (CuS), the hot holes generated in CuS via SP excitation can transfer to the VB of CdS, resulting in the lifetime prolonging of the charge carrier (9.2 μs) [70].

2.2.2 *At the plasmon-molecules interfaces*

The physical or chemical adsorbed molecules could also affect the separation of the plasmon-generated hot carriers. For an organic molecule, there exist energy level orbitals, including the highest occupied molecular orbital (HOMO) and the LUMO, in analog to the VB and CB in semiconductor. Similar to the case at the plasmon-semiconductor interface, the plasmon-generated hot carriers could in principle also be effectively separated at the plasmon-molecule interface, since the generated hot electrons/holes could transfer to the LUMO/HOMO of the adsorbed organic molecules, leaving opposite charges inside the plasmonic metal (Fig. 3) [44, 73]. If the plasmon-generated hot electrons are extracted by the adsorbed molecules, the hot holes leaved inside the plasmonic metal (Fig. 3(a)) may be utilized for direct oxidation of the plasmonic metal, leading to a morphological change on the metal surface [41]. On the other hand, if the generated hot holes transfer to the HOMO of the adsorbed organic molecules, the hot holes accumulated in organic molecules (Fig. 3(b)) can lead to a direct oxidation of the adsorbed or nearby molecules.

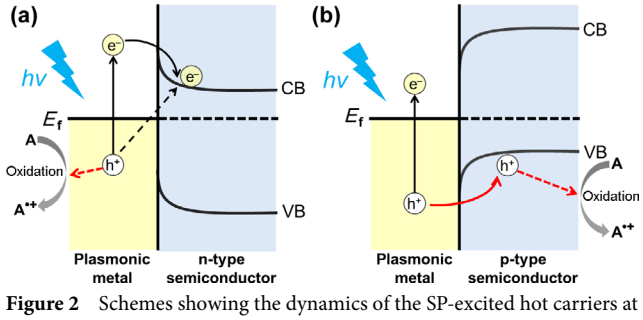

Figure 2 Schemes showing the dynamics of the SP-excited hot carriers at the interfaces between plasmonic metal and (a) n-type or (b) p-type semiconductor. E_f represents Fermi level. The black solid/dash arrow in panel (a) represents the indirect/direct transfer pathway for hot electrons.

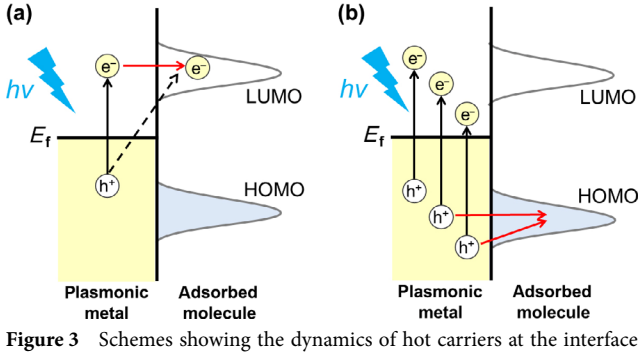

Figure 3 Schemes showing the dynamics of hot carriers at the interface between plasmonic metal and adsorbed molecules. E_f represents Fermi level. The solid/dash arrow in panel (a) represents the indirect/direct transfer pathway for hot electrons.

3 Hot hole-involved photochemistry at plasmon-semiconductor interfaces

A pure plasmonic metal or semiconductor usually possesses a narrow absorption band, which limits the utilization efficiency of sunlight in photocatalysis. Moreover, the photo-excited hot carriers may recombine easily in these pure structures, which make it difficult to make use of the hot carriers for redox reactions. One effective approach is to construct a heterostructure of plasmonic metal and semiconductor, in which an interfacial electric field exists at the plasmon-semiconductor interface, facilitating the effective separation of the generated hot electrons and holes. It has been reported that plasmonic metals (gold and silver) have been combined with many semiconductor materials, including TiO_2 [74], zinc oxide (ZnO) [75], CdS [76], molybdenum disulfide (MoS_2) [77], silver halides (AgX) [78], and bismuth oxide halides (BiOX) (X = Cl, Br, I) [79]. The obtained heterostructures showed enhanced photocatalytic performances, due to the improved charge separation.

It is fundamentally important to know the distribution of the hot electrons and holes at the plasmon-semiconductor heterostructure during a chemical reaction. Single-molecule fluorescence microscopy provides an effective way for this purpose [80, 81]. This technique helps to obtain a super-resolution image by determining the precise coordinates of the emission from every fluorophore with a localization algorism, followed by super-resolution reconstruction [82]. Using this technique, Fang and co-workers have revealed the distribution of the hot carriers under 532 nm light illumination in the Au-CdS heterostructure in which gold nanoparticles locate at the two tips of the CdS nanorod (n-type) [83]. It was found that the generated hot holes locate mainly at the gold tips, while the hot electrons locate along the CdS nanorod within a few tens of nanometers from the gold tips (Fig. 4), suggesting that the generated electrons via plasmon decay transfer to CdS nanorod and the holes remain inside gold nanoparticles.

In following parts, based on which side the hot holes remain, the photochemistry at the plasmon-semiconductor interfaces is divided into following two types.

3.1 Photochemistry involving the hot holes remaining inside plasmonic metal

3.1.1 *Etching of metals*

It has been demonstrated that the plasmon-generated hot holes left inside silver could be used directly for the etching of itself at the silver-titania (Ag-TiO_2) interface [41]. They deposited isolated silver nanocubes on TiO_2 film. Interestingly, the silver nanocubes were etched site-selectively under light illumination, and this site-selective etching is highly affected by the light wavelength of the illuminations. The bottom edges of the cubes are etched under 620–700 nm light illumination (Figs. 5(a) and 5(b)), while the top edges of the cubes are etched under 420 nm light illumination (Figs. 5(c) and 5(d)). This is due to the excitation of different plasmonic modes under these two light illuminations. Under 620–700 nm illumination, the proximal mode is excited and the electromagnetic field is localized at the bottom edges of the silver nanocube, where

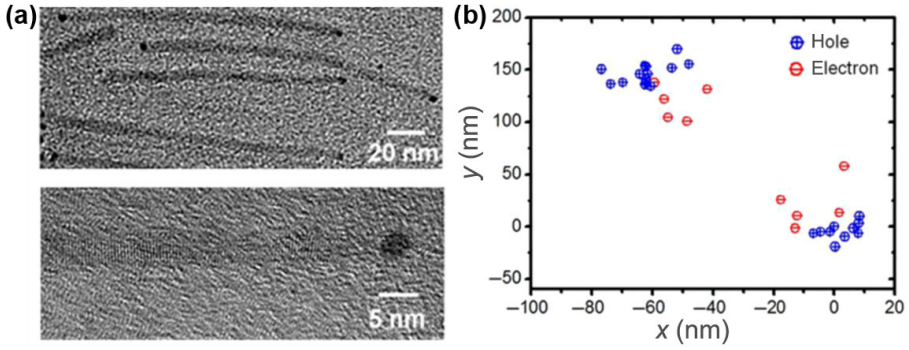

Figure 4 Distribution mapping of the plasmon-generated hot electrons and holes at the gold-tipped CdS nanorod. (a) A typical transmission electron microscopy (TEM) image of the gold-tipped CdS nanorods (top) and an enlarged image (bottom). (b) Super-resolution mapping of the plasmon-generated hot electrons and holes on a gold-tipped CdS nanorod under 532 nm light illumination. (Reprinted with permission from Ref. [83], © American Chemical Society 2014).

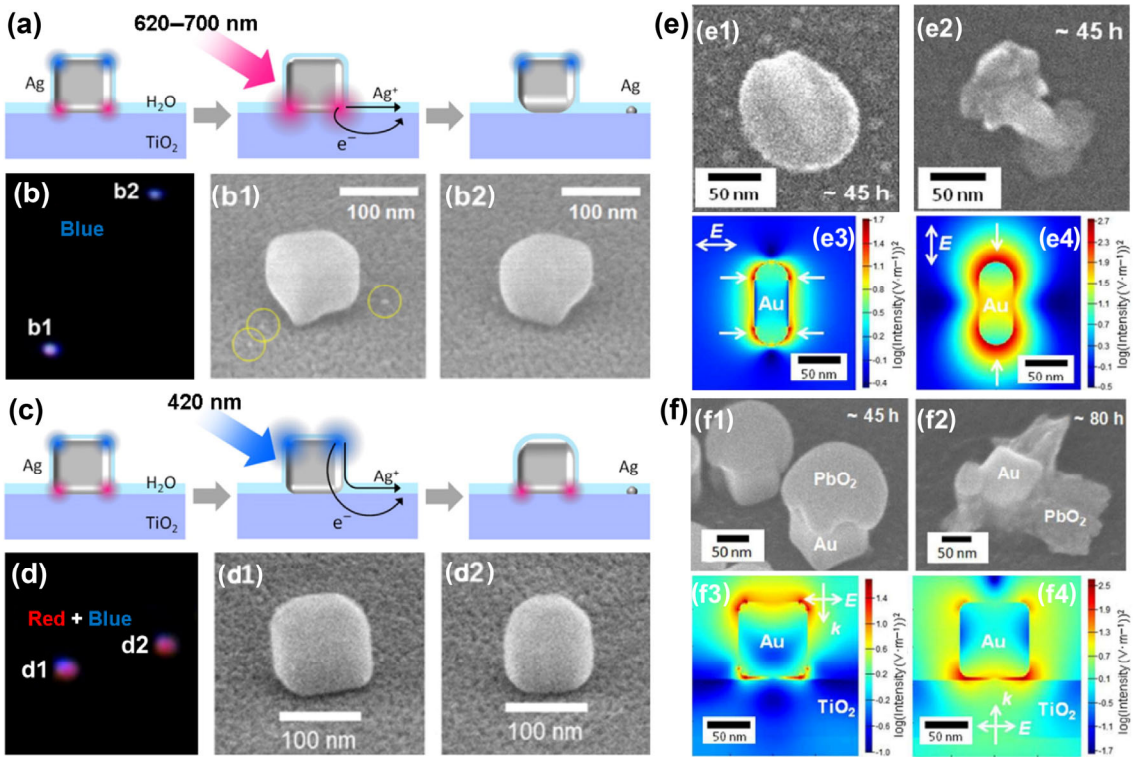

Figure 5 The etching of metal and deposition of oxide driven by the plasmon-generated hot holes. (a)–(d) Schematic illustrations ((a) and (c)), dark-field optical images ((b) and (d)) and scanning electron microscopy (SEM) images ((b1), (b2), (d1) and (d2)) of the site-selectively etched silver nanocubes on TO_2 surface under 620–700 and 420 nm illuminations, respectively. (e) SEM images and FDTD electric field simulations of the site-selectively deposited PbO_2 on the pre-coated gold nanorods on TiO_2 surface under 542 nm ((e1) and (e3)) and 728 nm ((e2) and (e4)) illuminations, which excite the transverse and longitudinal modes respectively. (f) SEM images and FDTD electric field simulations of the site-selectively deposited PbO_2 on the pre-coated gold nanocubes on TiO_2 surface under 542 nm ((f1) and (f3)) and 663 nm ((f2) and (f4)) illuminations, which excite the distal and proximal modes respectively. Panels (a)–(d) are reprinted with permission from Ref. [41], © American Chemical Society 2016. Panels (e) and (f) are reprinted with permission from Ref. [84], © The Royal Society of Chemistry 2018.

energetic hot holes are generated, explaining the selective etching of silver here. In contrast, under 420 nm illumination, the distal mode is excited and the electromagnetic field is more localized at the top edges of the nanocube, which leads to the selective etching of silver there.

3.1.2 *Deposition of oxides*

Besides etching, deposition of metal oxides could also be achieved with the aid of the plasmon-generated hot holes at the plasmon-semiconductor heterostructures. Tatsuma and co-workers have selectively deposited lead dioxide (PbO_2) on the gold nanoparticle-coated TiO_2 film [84]. It was found that the position of the PbO_2 deposition is dependent on both the shape of the gold nanoparticles and the wavelength of the light illumination. For gold nanospheres, PbO_2 is mainly deposited on the interface between gold nanospheres and TiO_2 film under 470–700 nm illumination, since the gold nanospheres are excited isotropically and the hot holes accumulate at the Au–TiO_2 interface. For gold nanorods, PbO_2 is selectively deposited on the sides and end caps of the gold nanorods under 542 and 728 nm illuminations, respectively (Fig. 5(e)), due to the excitation of the transverse and longitudinal modes in these two illuminations, respectively. For gold nanocubes, PbO_2 is deposited at the top and bottom of the gold nanocubes under 542 and 663 nm illuminations, respectively (Fig. 5(f)), due to the excitation of the distal and proximal modes in these two illuminations, respectively. In addition, the positions of the PbO_2 deposition are consistent with the distribution of the

localized electromagnetic field (where are called as hotspots) which has been obtained via the finite-difference time-domain (FDTD) simulation, implying that the hot holes are more effectively generated at these hotspots. Therefore, the SP excitation is crucial in the abovementioned selective deposition of PbO_2. Besides PbO_2, other metal oxides including chromium trioxide (Cr_2O_3) could also be selectively deposited with the aid of the plasmon-generated hot holes [85].

3.1.3 *Oxygen evolution reaction*

The plasmon-generated hot holes can also drive the oxygen evolution reaction (OER) [39, 86–89]. The heterostructures of gold and TiO_2 are often used for OER, since the generated hot holes in this system are energetic enough for the excitation of water molecules and the distinct Ti–O–Au interfacial structure is beneficial for water oxidation [85]. In detail, electron–hole pairs generate first via plasmon decay, and then the hot electrons transfer to TiO_2 by overcoming the Schottky barrier at the Au-TiO_2 interface, leaving the holes inside gold for oxidation of water to oxygen [90]. Li and co-workers have revealed that the water oxidation reaction happens at the interface of gold and TiO_2, suggesting the accumulation position of the hot holes (Fig. 6(a)) [85]. To further confirm this, the Au-TiO_2 heterostructure was photodeposited with Cr_2O_3 or PbO_2, which locates at the Au-TiO_2 interface and blocks up the sites for water oxidation. Therefore, the OER decelerates significantly, confirming that the water oxidation happens mainly at the Au-TiO_2 interface. The distribution of the hot holes have also been confirmed with the contact potential difference (CPD) and surface photovoltage (SPV) results via Kelvin probe force microscopy (KPFM) (Fig. 6(b)). These results show that the increase of SPV locates at the perimeter region between gold and TiO_2, indicating that the charge separation occurs and the holes accumulate at the Au-TiO_2 interface. Furthermore, Li group has also achieved overall water splitting by combining the Au-TiO_2 heterostructure with a hydrogen evolution catalyst, rhodium-doped strontium titanate (Rh-doped $SrTiO_3$) [91].

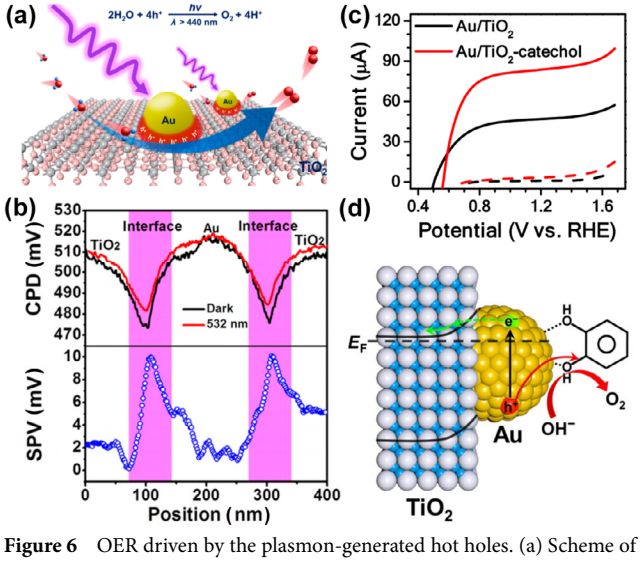

Figure 6 OER driven by the plasmon-generated hot holes. (a) Scheme of the site-specific hot hole accumulation and the water oxidation semi-reaction under visible light illumination. (b) CPD profiles (top) across the Au-TiO_2 heterostructure in dark (black line) and illuminated (red line) states; SPV profile (bottom) across the Au-TiO_2 heterostructure by subtracting above two CPD profiles. (The pink-colored zones represent the Au-TiO_2 interface regions). (c) Linear sweep voltammetry curves of the pristine (black curves) and catechol-modified (red curves) Au-TiO_2 heterostructures in dark (dashed curves) and under 470 nm light emitting diode (LED) illumination (solid curves). RHE stands for reversible hydrogen electrode. (d) Scheme illustrating the charge separation and water oxidation on the catechol-modified Au-TiO_2 heterostructure. Panels (a) and (b) are reprinted with permission from Ref. [85], © American Chemical Society 2017. Panels (c) and (d) are reprinted with permission from Ref. [93], © The Royal Society of Chemistry 2020.

Plasmonic heterostructures can also work in a photo-electrochemical (PEC) system for OER [91]. For example, Nam and co-workers designed a photoanode consisting of multilayer plasmonic heterostructures (layer-by-layer self-assembly of gold nanoparticles and TiO_2 nanoparticles) and copper-based oxygen evolution catalyst (Co-OEC). In this system, a large number of hot electrons are injected into the TiO_2 due to the large interfacial area, and the transportation of hot holes into electrolyte is largely improved due to the acceleration of water oxidation [92]. Recently, Wei and co-workers found, on Au-TiO_2 heterostructure, the catalytic activity is mainly limited by the recombination of the TiO_2-trapped hot holes with the transferred hot electrons [93]. By adsorbing catechol molecules on gold, the catalytic activity of the Au-TiO_2 heterostructure is largely enhanced. In the water oxidation reaction carried out in a photoelectrochemical cell, the photocurrent at 1.2 V_{RHE} increases from 47 to 84 μA (Fig. 6(c)). The reaction order of the TiO_2-trapped holes drops by four times on the catechol-adsorbed Au-TiO_2 heterostructure than that on pristine one, indicating that the adsorbed catechol molecules on Au-TiO_2 heterostructures could trap and stabilize the hot holes directly on gold, leading to an effective separation with the transferred hot electrons on TiO_2 surface (Fig. 6(d)).

3.1.4 *Oxidation of organic molecules*

The plasmon-generated hot holes can also drive the oxidation of organic molecules, such as alcohol [94–98] and formic acid [99–105], at the plasmon-semiconductor interfaces, making plasmonic heterostructures promising in green synthesis of organic molecules.

Benzylamine can be photo-oxidized to benzyl-phenylmethanimine with the assistance of the Au-TiO_2 heterostructure [106]. The plasmon-generated hot holes with enough energy could transfer to the HOMO of the adsorbed benzylamine molecules, initiating the formation of benzylamine radical cations. These radical cations react with the superoxide radicals activated by the plasmon-generated hot electrons, producing benzyl-phenylmethanimine (Fig. 7(a)). It is worth noting that the reaction efficiency could be improved by introducing plasmonic broadband absorber. By forming multi-layer stack of plasmonic nanoparticles or combing assembled plasmonic nanoparticles with metal mirror, the light absorption of the samples could be largely enhanced due to the existence of multiple reflections [107, 108]. Gomez and co-workers have developed a plasmonic broadband absorber composed of gold nanoparticles, TiO_2 film intermediate layer, and gold mirror, which exhibits a strong light absorption of ~ 94% at 580 nm. They found that, under visible light illumination, the benzylamine oxidation efficiency increases 29 folds on the broadband absorber compared with that on gold nanoparticle-coated TiO_2 film (Fig. 7(b)) [106].

The plasmon-generated hot holes could also be used for selective oxidation of benzyl alcohol to benzaldehyde. Zhang and co-workers have demonstrated this oxidation on gold nanoparticle-coated bismuth oxychloride (BiOCl) micro sphere under visible light illumination (Fig. 7(c)) [98]. It was proposed that the plasmon-generated hot holes leave inside gold and oxidize benzyl alcohol to carbon center radicals, while the hot electrons transferred to BiOCl react with the adsorbed oxygen (O_2), producing superoxide radicals. These two types of radicals

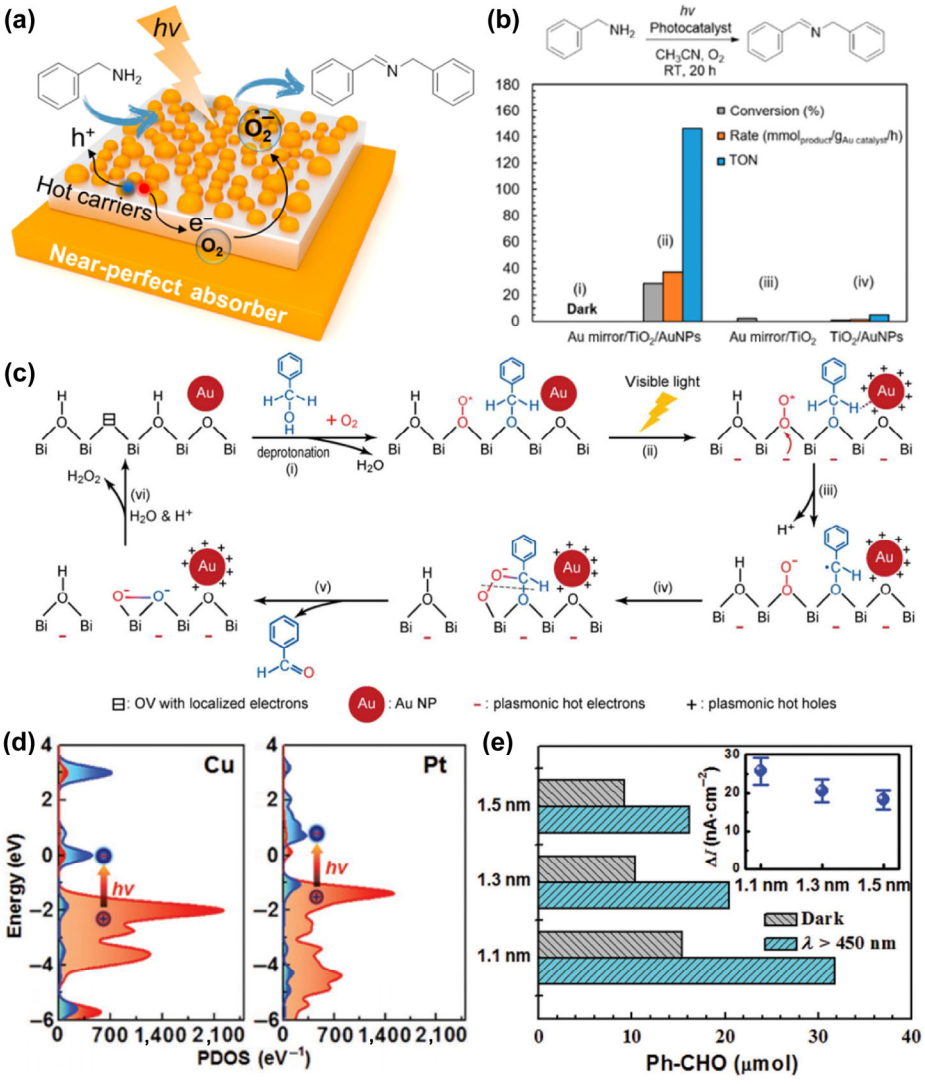

Figure 7 Organic transformations driven by the plasmon-generated hot holes. (a) Schematic structure of plasmonic broadband absorber and the mechanism of benzylamine oxidation. (b) Conversion percentages, reaction rates and turn over numbers (TONs) of the photocatalytic benzylamine oxidation on the plasmonic broadband absorber in dark (i) and under LED illumination (ii), on the TiO_2 thin film supported by gold mirror (iii), and on the TiO_2 thin film coated with gold nanoparticles (iv) under LED illumination, respectively. (c) Proposed mechanism for the selective oxidation of benzyl alcohol on gold nanoparticle-coated BiOCl crystals with oxygen vacancies. (d) The spectra of PDOS for model Cu_{13} (left) and Pt_{13} (right) clusters, in which PDOS of d and orbits are marked in orange red and ultramarine color, respectively. The generation of hot carriers is also included, as electrons near Fermi level are excited from d to sp orbitals. (e) Amounts of the formed benzaldehyde catalyzed by the PtCu/TiO_2-NB with different cluster sizes (1.1, 1.3 and 1.5 nm) in dark (gray) and under visible light illumination (cyan). Inset shows the photocurrent responses of the catalysts with different cluster sizes under visible light illumination. Panels (a) and (b) are reprinted with permission from Ref. [106], © American Chemical Society 2018. Panel (c) is reprinted with permission from Ref. [98], © American Chemical Society 2017. Panels (d) and (e) are reprinted with permission from Ref. [109], © Zhang, L. C. et al. 2017.

then undergo ring addition, producing benzaldehyde. They also found that the efficiency of benzyl alcohol oxidation is further improved for ten times if the BiOCl crystals are replaced with the ones with oxygen vacancies.

The selective oxidation of benzyl alcohol could also be realized on the platinum-copper (PtCu) alloy nanoclusters-coated TiO_2 nanobelts (PtCu/TiO_2-NB) [109]. It was found that, under visible light illumination, the PtCu/TiO_2-NB structure exhibits a higher catalytic activity, up to three times, compared with the platinum nanoclusters-coated TiO_2 nanobelts (Pt/TiO_2-NB), due to the synergistic effect between platinum and copper. The projected density of state (PDOS) of the d orbital in copper is larger than that in platinum (Fig. 7(d)); therefore, the copper atoms in PtCu cluster can be more effectively excited via inter-band transition, generating hot electrons and holes. The hot electrons transfer to TiO_2, while the hot holes leave inside the alloy cluster, promoting the catalytic oxidation of benzyl alcohol. Moreover, the catalytic performance of PtCu/TiO_2-NB decreases remarkably with an increase in the size of the alloy cluster (Fig. 7(e)), which is possibly due to the fact that the hot holes are very short in lifetime. Therefore, the hot holes in a smaller sized alloy cluster have a better chance to reach the surface for chemical reaction.

3.2 Photochemistry involving the hot holes remaining inside semiconductor

The plasmon-generated hot holes can also be extracted into the semiconductor side on the metal-semiconductor heterostructures. Atwater and co-workers have reported a heterostructure of gold and p-type gallium nitride (p-GaN) as photocathode for effective capture and conversion of hot holes [110]. Under light illumination, electron-hole pairs form via plasmon decay, and the holes with enough energy could overcome the Schottky barrier and transfer to p-GaN (Fig. 8(a)). Due to this transportation of hot holes, an increased open-circuit voltage

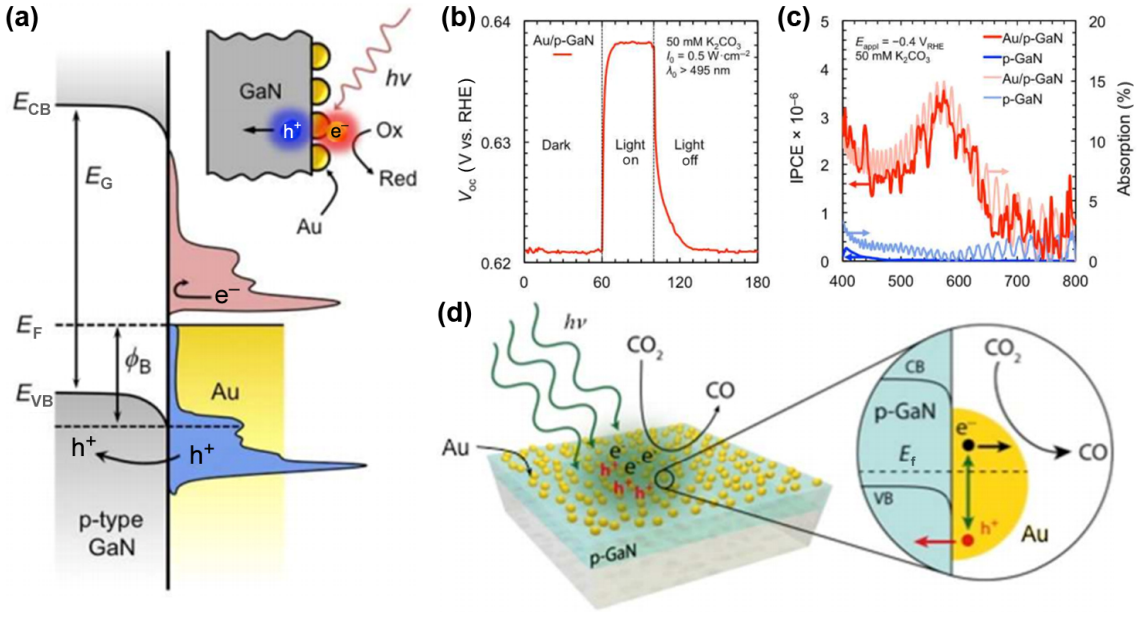

Figure 8 Collection and utilization of the plasmon-generated hot holes at the heterostructure of gold and p-GaN. (a) Scheme showing the hot hole collection at the Au/p-GaN interface. E_{CB}: the edge of conduction band, E_{VB}: the edge of valence band, E_G: band gap, E_F: Fermi level, Φ_B: interfacial Schottky barrier. (b) Open-circuit voltages (V_{oc}) of the Au/p-GaN photocathode before, during and after the visible-light illumination. (c) IPCE of the p-GaN photocathode (blue) and the one coated with AuNPs (red). The absorption spectra of these two photocathodes are also plotted together for easy comparison. (d) Scheme showing that the hot electrons left in gold could drive the selective reduction of CO_2 to CO. (Reprinted with permission from Ref. [110], © American Chemical Society 2018).

has been observed (Fig. 8(b)). Furthermore, the wavelength dependency in incident photon-to-charge conversion efficiency (IPCE) is consistent with the plasmon extinction spectrum of the gold nanoparticles (Fig. 8(c)), indicating the importance of SP excitation in energy conversion. Moreover, the hot electrons left in gold can drive the selective reduction of CO_2 to carbon monoxide (CO) (Fig. 8(d)), producing an energy-rich chemical compound.

4 Hot hole-involved photochemistry at plasmon-molecule interfaces

As discussed, the energy levels of organic molecules are in analogy to the band structures of semiconductors. When plasmonic nanostructures were adsorbed physically or chemically with organic molecules, effective charge separation could also be achieved at the plasmon-molecule interfaces. The plasmon-generated hot carriers with suitable energy could transfer to the HOMO or LUMO of the adsorbed molecules. There are two scenarios here: 1) hot holes accumulate inside the adsorbed molecules, which could drive chemical reactions of the adsorbed or nearby molecules; 2) hot holes accumulate inside the plasmonic metal, which could drive the direct oxidation of the plasmonic metal itself or the chemical reaction of nearby molecules. Based on this, the photochemical reactions involving the hot holes at plasmon-molecule interfaces are divided into following two categories.

4.1 Chemical reactions involving the hot holes accumulated inside adsorbed molecules

4.1.1 4-ATP to DMAB conversion

It has been demonstrated that 4-aminothiophenol (4-ATP) could be oxidized to p,p'-dimercaptoazobenzene (DMAB) on silver surface under light illumination. As known, plasmonic nanostructure can lead to an extremely localized electromagnetic field [79, 111, 112], which could result to an enhancement of Raman scattering, also called as surface-enhanced Raman scattering (SERS) [113]. SERS spectroscopy could be employed for effective identification of chemical reactions. It was reported that new bands different from the characteristic vibrations of 4-ATP showed up during SERS measurements on silver surface, which were initially attributed to the non-fully symmetric vibration (b_2 mode) of 4-ATP [114]. Afterward, by using density functional theory (DFT), Tian and co-workers proposed that 4-ATP can be converted to DMAB on silver surface *via* a catalytic coupling reaction [115]. Therefore, the so-called b_2 mode actually derives from the DMAB molecules. Since then, many experimental works have confirmed that the DMAB molecules are produced on plasmonic metals via the oxidation of 4-ATP molecules [116–121], which is assisted by the SP excitation. The plasmon-generated hot holes transfer to the HOMO of the adsorbed 4-ATP molecules, which trigger the coupling reaction of 4-ATP molecules to form DMAB (Fig. 9(a)) [122–124]. Note that SERS contributes a lot to the observation of the 4-ATP to DMAB conversion by largely enhancing the signals of molecular vibrations. Recently, SERS technology has been intensively used for studying the kinetics of many catalytic reactions [125].

4.1.2 Glucose oxidation

Li and co-workers have reported a speeded up oxidation of glucose with the assistance of SP [126]. Glucose can be oxidized to gluconic acid with the existence of 13 nm spherical gold nanoparticles (AuNPs) even in dark condition; however, if SPs are excited by illuminating the samples with 532 nm light, the yield of glucose oxidation doubles compared with that in dark state (Fig. 9(b)). Moreover, the glucose oxidation reaction can be deactivated by keeping the reaction in dark state for 60 min, and the reaction can also be reactivated under light illumination (Fig. 9(c)). It was found that the plasmon-generated hot holes are crucial in this glucose oxidation, which was confirmed by the DFT calculation and the extended X-ray absorption fine structure. The results suggest that the plasmon-generated hot

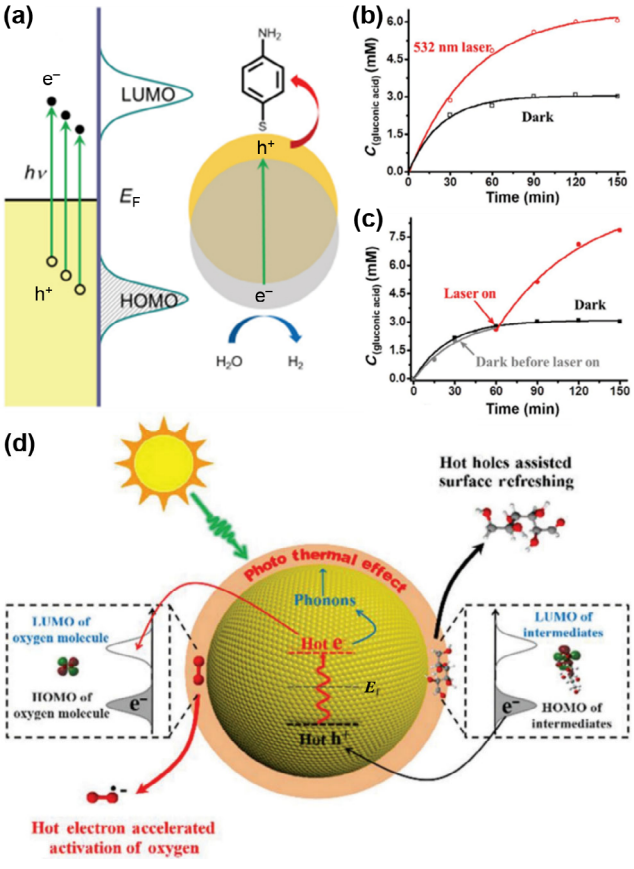

Figure 9 Oxidations of 4-ATP and glucose driven by the plasmon-generated hot holes. (a) Proposed mechanism for the 4-ATP oxidation driven by the plasmon-generated hot holes. (b) The catalytic glucose oxidation on gold nanoparticle surface in present (red) and absent (black) of 532 nm laser illumination. (c) The catalytic glucose oxidation on gold nanoparticle surface in dark for one hour followed by 532 laser illumination (marked with arrow). (d) Scheme illustrating the role of the plasmon-generated hot electrons and holes in glucose oxidation. Panel (a) is reprinted with permission from Ref. [123], © Shanghai Institute of Organic Chemistry, Chinese Academy of Sciences 2014. Panels (b)–(d) are reprinted with permission from Ref. [126], © Wiley-VCH Verlag GmbH & Co. KGaA, Weinheim 2018.

electrons can transfer from gold to the adsorbed O_2, while the hot holes locate deep under the Fermi level of gold. These hot holes are energetic enough to transfer to the HOMO of the glucose oxidation intermediates, driving their chemical conversion. Moreover, the adsorption energy of gluconic acid (0.2–0.3 eV) is much lower than that of the intermediate molecule (about 3 eV) on gold surface, thereby promoting the desorption of product molecules from the gold surface and liberating the reaction sites. In short, the key to the observed enhancement of catalytic performance is the plasmon-induced hot electrons and hot holes, in which hot holes drive the conversion of intermediate to products and reactivate the catalytic surface (Fig. 9(d)).

4.1.3 *Citrate oxidation*

Brus has reported that the excited SPs can help oxidizing the adsorbed citrate ions and reduce the silver ions in sodium citrate-stabilized silver colloid [127]. Later, the plasmon-generated hot holes are proposed responsible for the oxidation of the adsorbed citrate ions [128]. The dynamics of the hot holes in citrate oxidation were later studied in an electrochemical cell [129]. In this cell, the Au@SiO_2@Au core–shell nanoparticles were deposited on indium tin oxide (ITO) surface as working electrode (Fig. 10(a)). When the electrode is illuminated with a 2.36 eV laser beam, a drop in open-circuit photovoltage can be observed, indicating an accumulation of electrons in the Au@SiO_2@Au core–shell nanoparticles and transferring of holes to the adsorbed citrate ions (Fig. 10(b)). In this case, the excitation of the d-band electrons produces a large number of high-energy holes near the edge of the d band, and these energetic holes easily transfer to the HOMO of the citrate ions (Fig. 10(c)). In contrast, if the structure is excited with a 1.65 eV laser, only cold holes near the Fermi level or warm holes below the Fermi level may be generated. The cold holes cannot transfer to the HOMO of the citrate ions due to the energy insufficiency, while the warm holes are energetic enough to transfer to the HOMO of the citrate ions. Therefore, an improved reactivity can also be observed with 1.65 eV excitation, yet the measured photovoltage drop, calculated far-field absorption, and hot carrier-adsorbate overlap are lower than those in the condition of 2.3 eV excitation.

4.1.4 *Dye degradation*

Dye degradation could also be realized with the assistance of the plasmon-generated hot holes [130, 131]. Hu and co-workers have studied the role of the hot holes in the degradation of rhodamine 6G (R6G) on the silver-decorated copper nanoparticles [132]. As a control, the R6G degradation on bare copper nanoparticles was first carried out. In this case, R6G could be effectively degraded due to the dye sensitization effect. However, if the copper nanoparticles are decorated with silver, the R6G degradation is significantly retarded (degradation dropped from 97.3% to 83.3%), which is attributed to the weakening of dye sensitization. For bare copper nanoparticle, the generated hot electrons can transfer to the adsorbed O_2, generating oxygen radical (O_2^-); while the holes transfer to the excited R6G molecule, maintaining the charge neutrality. This dye sensitization promotes the formation of O_2^- and the oxidation of R6G. However, the doped silver can also be excited to generate hot electrons, which could transfer to copper and weaken the dye sensitization effect, resulting in a reduction in photocatalytic efficiency. This result shows that the bimetallic plasmonic structure may not necessarily promote the efficiency of the catalytic reaction.

4.2 Chemical reactions involving the hot holes accumulated inside plasmonic metal

When the plasmon-generated hot electrons were extracted, the hot holes may accumulate inside the metal itself. These accumulated hot holes could lead to an oxidation of the metal itself if the energy of the holes was high enough.

4.2.1 *Metal dissolution*

Uji-i and co-workers have found that silver nanowires could be selectively dissolved with the presence of certain Raman probe molecules under laser irradiation (Figs. 11(a) and 11(b)) [133], however the mechanism was not clear at that moment. We believe this selective dissolution of silver can be attributed to the accumulation of the plasmon-generated hot holes inside silver. Note that gold cannot be dissolved in the same condition, possibly due to the limited energy of the generated hot holes, which is unable to oxidize gold. This could be overcome by applying a bias. Landes and co-workers have found that the gold nanoparticles coated on an electrode could be dissolved at a bias of 0.48 V [134]. In this case, the chloride ions in the electrolyte solution can be adsorbed onto the gold surface. Due to the existence of the chloride ions, gold could be dissolved even in dark state; however, the dissolution accelerates dramatically when the structure is irradiated with a white-light laser (Fig. 11(c)). In addition, the dissolution rate depends

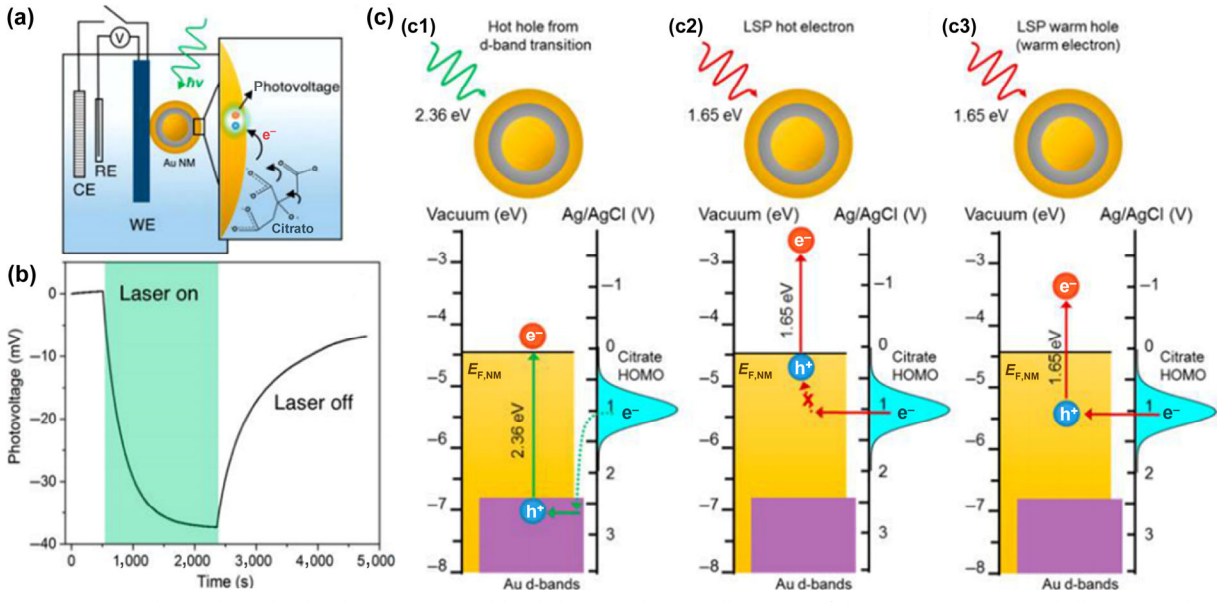

Figure 10 Citrate oxidation driven by the plasmon-generated hot holes. (a) Schematic illustration of the Au@SiO_2@Au core–shell nanoparticles coated electrode in a three-electrode electrochemical cell in open-circuit condition. Under laser illumination, electron–hole pairs are generated via nonradiative plasmon decay. The hot holes participate in the photooxidation of the citrate ions on surface, while the hot electrons are collected on the nanoparticle surface, resulting in a measurable photocharging. (b) Open-circuit potential change on Au@SiO_2@Au core-shell nanoparticles coated electrode before, during, and after 550 nm laser irradiation. (c) Energy band diagrams describing possible mechanisms for citrate oxidation driven by the plasmon-generated hot holes. (c1) The photo excitation with 2.36 eV light results in the formation of hot holes in d band of gold, which could transfer to the HOMO of the citrate ions, triggering its oxidation. (c2) The photo excitation with 1.65 eV light may produce hot electrons but cold holes, which remain near Fermi level of gold and cannot transfer to the HOMO of the citrate ions. (c3) Warm holes may also be generated via plasmon decay with the 1.65 eV light excitation, and these warm holes have enough energy to transfer to the HOMO of the citrate ions. (Reprinted with permission from Ref. [129], © American Chemical Society 2017).

on the power and wavelength of the incident light, suggesting a crucial role of SP excitation in gold dissolution (Fig. 11(d)). It has been found that the hot holes generated via the inter-band excitation are more effective than the ones generated around the Fermi level in promoting the gold dissolution, which is consistent with many studies [129, 135, 136]. The authors have proposed that the plasmon-generated hot holes accumulate inside gold and drive the oxidation of the gold. The existence of chloride ions could lead to the formation of soluble Au(I) complexes to accelerate the gold dissolution process.

4.2.2 *Photo-recycling of metal*

With the presence of certain inorganic ions, the plasmon-mediated reaction may be different. Schlucker and co-workers studied the reduction of the 4-nitrothiophenol (4-NTP) molecules grafted on the surface of core-satellite silver superstructure in presence of protons and halides [137]. When the superstructure is excited with a resonant light, electron-hole pairs are generated, and then the hot electrons transfer to 4-NTP and participate in 4-NTP reduction, while the hot holes leave inside the silver superstructure and combine with the chloride ions on silver surface, forming photosensitive silver chloride (AgCl). This AgCl can decompose into silver and chlorine radical *via* photodissociation. Then, the electron transfer from Cl^- to the silver catalyst, and more hot electrons can be provided for the reduction of 4-NTP. Therefore, the chloride ions help the recycling of silver atoms and act as electron donors for more effective accumulation of hot holes.

5 Conclusion and outlook

In conclusion, the plasmon-generated hot holes have been proven effective in driving many photochemical reactions, including organic transformation, metal etching, oxide deposition, and oxygen evolution. In this review, we first discussed the generation and energy distribution of the hot carriers in several plasmonic materials. The energy distribution of the generated hot carriers is highly dependent on the intrinsic characteristics of the plasmonic nanostructures (e.g. type, size, shape) and the external excitation parameters. If the generated hot holes have enough energy, they could be utilized in many chemical reactions. Due to the very short lifetime of the hot holes, effective separation and collection of these hot holes is a key to high efficient chemical conversions, which can be realized by constructing an interface with semiconductor or adsorbing organic molecules with a suitable energy band/level structure. At the plasmon-semiconductor or plasmon-molecule interface, many oxidation reactions have been realized with the assistance of the plasmon-generated hot holes. However, the potential of the plasmon-generated hot holes in chemical conversions has not been fully explored due to the huge mismatch between their femto- to picosecond lifetime and the time scale of chemical reactions, which is usually in a range of millisecond or sub-millisecond. Therefore, much more work needs to be done and the photochemistry involving plasmon-generated hot holes may play a crucial role in energy conversions and artificial syntheses in near future.

Even though the plasmon-generated hot holes have a great potential in driving many chemical reactions, there are still many challenges remaining. (1) The dynamics of the hot holes and the mechanism of their utilization in chemical reactions are still unclear. The lifetime of the holes is in the range of femtosecond to picosecond, making it difficult to investigate experimentally. Recently, ultrafast spectroscopy has been employed in studying the relaxation and transfer processes of the hot holes [70], showing its great potentials. However, there are still many more processes left in fuzziness, and more techniques, especially the ones with high spatial resolutions,

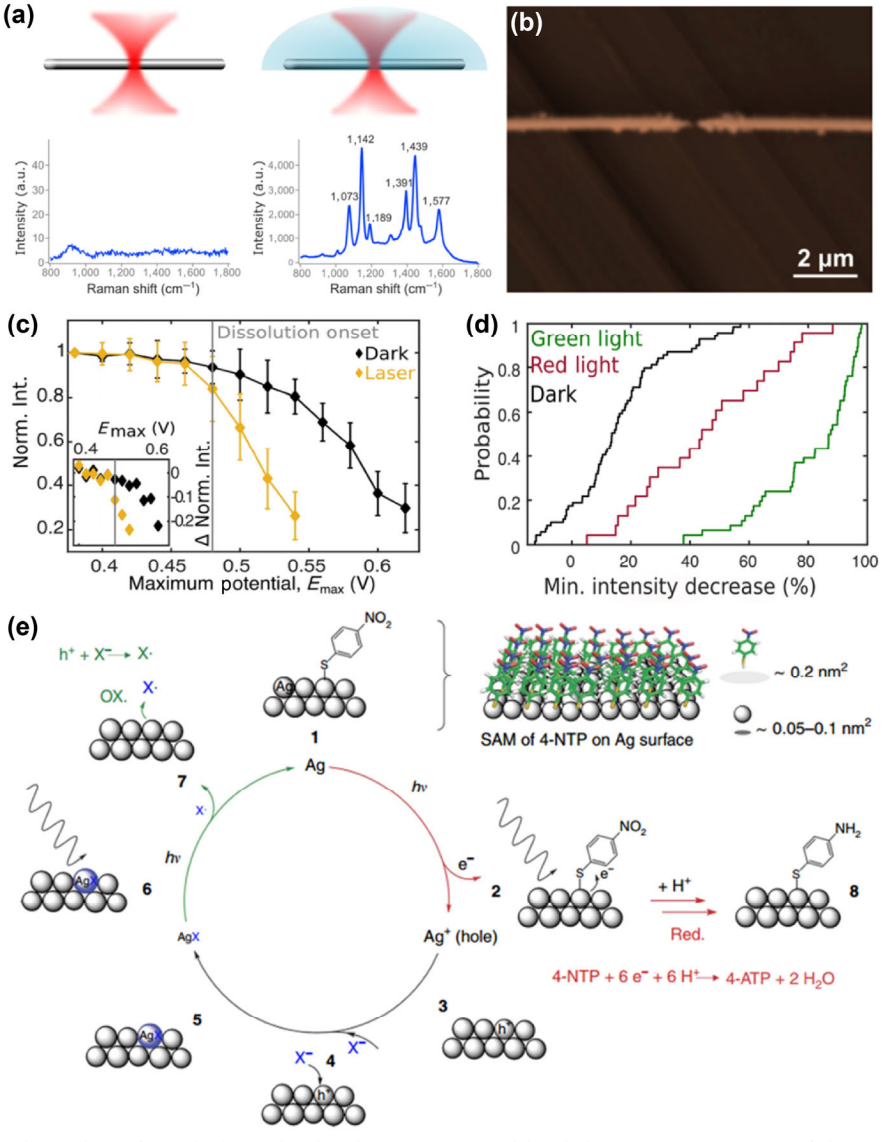

Figure 11 Dissolution and recycling of metals driven by the plasmon- generated hot holes. (a) Raman spectra of the 4-ATP-functionalized silver nanowire measured at air–glass and water–glass interfaces, indicating a light-induced dissolution of silver in water. (b) SEM image of the silver nanowire after the site-specific dissolution. (c) Scattering intensity change of the gold nanorods deposited on an electrode with the increase of electric potential in dark condition (black curve) and under white-light laser illumination (yellow curve). Inset shows the normalized intensity change. The vertical gray line indicates the onset potential for gold dissolution. (d) Cumulative probabilities of the final scattering intensity decreases for the gold nanorods in dark (black curve) and under red (red curve) or green (green curve) light illuminations. (e) Schematic illustration of the silver recycling with the assistance of the adsorbed 4-NTP molecules. Panels (a) and (b) are reprinted with permission from Ref. [133], © American Chemical Society 2017. Panels (c) and (d) are reprinted with permission from Ref. [134], © American Chemical Society 2019. Panel (e) is reprinted with permission from Ref. [137], © Macmillan Publishers Limitted 2015.

need to be developed or introduced in the study of plasmonic catalysis. (2) The separation efficiency of hot carriers and the utilization efficiency of hot holes are still low. To further improve these efficiencies, new strategies need to be developed, among which designing and fabricating asymmetric heterostructures (also called Janus nanostructure) may become an effective way. (3) Although many chemical reactions have been realized with the assistance of the plasmon-generated hot holes, it is still necessary and urgent to explore more chemical reactions (especially the ones useful and important in industry) which could be driven by the plasmon-generated hot holes. (4) By constructing plasmon-semiconductor or plasmon-molecule interface, the oxidation ability of the hot holes could be fine-tuned, making it theoretically possible to realize chemical reactions with high selectivity. However, this field is still in its infancy, and much more theoretical and experimental work needs to be done.

Acknowledgements

This work was supported by the National Natural Science Foundation of China (No. 11974180), Key University Science Research Project of Jiangsu Province (No. 17KJA150005), Six Talent Peaks Project in Jiangsu Province (No. XCL-038) and Postgraduate Research & Practice Innovation Program of Jiangsu Province (No. KYCX20_1060).

References

[1] Hoffmann, M. R.; Martin, S. T.; Choi, W.; Bahnemann, D. W. Environmental applications of semiconductor photocatalysis. *Chem. Rev.* **1995**, *95*, 69–96.

[2] Herrmann, J. M. Heterogeneous photocatalysis: Fundamentals and applications to the removal of various types of aqueous pollutants. *Catal. Today* **1999**, *53*, 115–129.

[3] Chen, H. M.; Chen, C. K.; Liu, R. S.; Wu, C. C.; Chang, W. S.; Chen, K. H.; Chan, T. S.; Lee, J. F.; Tsai, D. P. A new approach to solar hydrogen production: A ZnO-ZnS solid solution nanowire array photoanode. *Adv. Energy Mater.* **2011**, *1*, 742–747.

[4] Chen, H. M.; Chen, C. K.; Lin, C. C.; Liu, R. S.; Yang, H.; Chang, W. S.; Chen, K. H.; Chan, T. S.; Lee, J. F.; Tsai, D. P. Multi-bandgap-sensitized ZnO nanorod photoelectrode arrays for water splitting: An X-ray absorption spectroscopy approach for the electronic evolution under solar illumination. *J. Phys. Chem. C* **2011**, *115*, 21971–21980.

[5] Su, Y. H.; Straathof, N. J. W.; Hessel, V.; Noël, T. Photochemical transformations accelerated in continuous-flow reactors: Basic concepts and applications. *Chem.–Eur. J.* **2014**, *20*, 10562–10589.

[6] Fujishima, A.; Honda, K. Electrochemical photolysis of water at a semiconductor electrode. *Nature* **1972**, *238*, 37–38.

[7] Zhai, X. T.; Li, Z. Y.; Lu, Z. C.; Wang, G. L.; Li, P.; Gao, Y. Q.; Huang, X.; Huang, W.; Uji-i, H.; Lu, G. Synthesis of 42-faceted bismuth vanadate microcrystals for enhanced photocatalytic activity. *J. Colloid Interface Sci.* **2019**, *542*, 207–212.

[8] Yi, R. H.; Wang, Y. L.; Zhou, X.; Li, Z. Y.; Zhang, C. Y.; He, C. Y.; Li, H.; Gao, Y. Q.; Huang, X.; Lu, G. Crack formation on crystalline bismuth oxychloride thin square sheets by using a wet-chemical method. *ChemNanoMat* **2020**, *6*, 759–764.

[9] Rosi, N. L.; Mirkin, C. A. Nanostructures in biodiagnostics. *Chem. Rev.* **2005**, *105*, 1547–1562.

[10] Reinhard, B. M.; Sheikholeslami, S.; Mastroianni, A.; Alivisatos, A. P.; Liphardt, J. Use of plasmon coupling to reveal the dynamics of DNA bending and cleavage by single ecorv restriction enzymes. *Proc. Natl. Acad. Sci. USA* **2007**, *104*, 2667–2672.

[11] Sönnichsen, C.; Reinhard, B. M.; Liphardt, J.; Alivisatos, A. P. A molecular ruler based on plasmon coupling of single gold and silver nanoparticles. *Nat. Biotechnol.* **2005**, *23*, 741–745.

[12] Haes, A. J.; Van Duyne, R. P. A nanoscale optical biosensor: Sensitivity and selectivity of an approach based on the localized surface plasmon resonance spectroscopy of triangular silver nanoparticles. *J. Am. Chem. Soc.* **2002**, *124*, 10596–10604.

[13] Elghanian, R.; Storhoff, J. J.; Mucic, R. C.; Letsinger, R. L.; Mirkin, C. A. Selective colorimetric detection of polynucleotides based on the distance-dependent optical properties of gold nanoparticles. *Science* **1997**, *277*, 1078–1081.

[14] Seh, Z. W.; Liu, S. H.; Low, M.; Zhang, S. Y.; Liu, Z. L.; Mlayah, A.; Han, M. Y. Janus Au-TiO_2 photocatalysts with strong localization of plasmonic near-fields for efficient visible-light hydrogen generation. *Adv. Mater.* **2012**, *24*, 2310–2314.

[15] Thomann, I.; Pinaud, B. A.; Chen, Z. B.; Clemens, B. M.; Jaramillo, T. F.; Brongersma, M. L. Plasmon enhanced solar-to-fuel energy conversion. *Nano Lett.* **2011**, *11*, 3440–3446.

[16] Awazu, K.; Fujimaki, M.; Rockstuhl, C.; Tominaga, J.; Murakami, H.; Ohki, Y.; Yoshida, N.; Watanabe, T. A plasmonic photocatalyst consisting of silver nanoparticles embedded in titanium dioxide. *J. Am. Chem. Soc.* **2008**, *130*, 1676–1680.

[17] Linic, S.; Aslam, U.; Boerigter, C.; Morabito, M. Photochemical transformations on plasmonic metal nanoparticles. *Nat. Mater.* **2015**, *14*, 567–576.

[18] Ueno, K.; Misawa, H. Surface plasmon-enhanced photochemical reactions. *J. Photochem. Photobiol. C Photochem. Rev.* **2013**, *15*, 31–52.

[19] Maier, S. A.; Atwater, H. A. Plasmonics: Localization and guiding of electromagnetic energy in metal/dielectric structures. *J. Appl. Phys.* **2005**, *98*, 011101.

[20] Cushing, S. K.; Li, J. T.; Meng, F. K.; Senty, T. R.; Suri, S.; Zhi, M. J.; Li, M.; Bristow, A. D.; Wu, N. Q. Photocatalytic activity enhanced by plasmonic resonant energy transfer from metal to semiconductor. *J. Am. Chem. Soc.* **2012**, *134*, 15033–15041.

[21] Lee, M. G.; Moon, C. W.; Park, H.; Sohn, W.; Kang, S. B.; Lee, S.; Choi, K. J.; Jang, H. W. Dominance of plasmonic resonant energy transfer over direct electron transfer in substantially enhanced water oxidation activity of $BiVO_4$ by shape-controlled Au nanoparticles. *Small* **2017**, *13*, 1701644.

[22] Fedoruk, M.; Meixner, M.; Carretero-Palacios, S.; Lohmüller, T.; Feldmann, J. Nanolithography by plasmonic heating and optical manipulation of gold nanoparticles. *ACS Nano* **2013**, *7*, 7648–7653.

[23] Chaunchaiyakul, S.; Setiadi, A.; Krukowski, P.; Catalan, F. C. I.; Akai-Kasaya, M.; Saito, A.; Hayazawa, N.; Kim, Y.; Osuga, H.; Kuwahara, Y. Nanoscale dehydrogenation observed by tip-enhanced Raman spectroscopy. *J. Phys. Chem. C* **2017**, *121*, 18162–18168.

[24] Denzler, D. N.; Frischkorn, C.; Hess, C.; Wolf, M.; Ertl, G. Electronic excitation and dynamic promotion of a surface reaction. *Phys. Rev. Lett.* **2003**, *91*, 226102.

[25] Sundararaman, R.; Narang, P.; Jermyn, A. S.; Goddard III, W. A.; Atwater, H. A. Theoretical predictions for hot-carrier generation from surface plasmon decay. *Nat. Commun.* **2014**, *5*, 5788.

[26] Baffou, G.; Bordacchini, I.; Baldi, A.; Quidant, R. Simple experimental procedures to distinguish photothermal from hot-carrier processes in plasmonics. *Light Sci. Appl.* **2020**, *9*, 108.

[27] Dong, Y. Y.; Su, Y. L.; Du, L. L.; Wang, R. F.; Zhang, L.; Zhao, D. B.; Xie, W. Plasmon-enhanced deuteration under visible-light irradiation. *ACS Nano* **2019**, *13*, 10754–10760.

[28] Zhan, C.; Wang, Z. Y.; Zhang, X. G.; Chen, X. J.; Huang, Y. F.; Hu, S.; Li, J. F.; Wu, D. Y.; Moskovits, M.; Tian, Z. Q. Interfacial construction of plasmonic nanostructures for the utilization of the plasmon-excited electrons and holes. *J. Am. Chem. Soc.* **2019**, *141*, 8053–8057.

[29] Li, W.; Miao, J. J.; Peng, T. H.; Lv, H.; Wang, J. G.; Li, K.; Zhu, Y.; Li, D. Single-molecular catalysis identifying activation energy of the intermediate product and rate-limiting step in plasmonic photocatalysis. *Nano Lett.* **2020**, *20*, 2507–2513.

[30] Zhai, Y. M.; DuChene, J. S.; Wang, Y. C.; Qiu, J. J.; Johnston-Peck, A. C.; You, B.; Guo, W. X.; DiCiaccio, B.; Qian, K.; Zhao, E. W. et al. Polyvinylpyrrolidone-induced anisotropic growth of gold nanoprisms in plasmon-driven synthesis. *Nat. Mater.* **2016**, *15*, 889–895.

[31] White, J. L.; Baruch, M. F.; Pander III, J. E.; Hu, Y.; Fortmeyer, I. C.; Park, J. E.; Zhang, T.; Liao, K.; Gu, J.; Yan, Y. et al. Light-driven heterogeneous reduction of carbon dioxide: Photocatalysts and photoelectrodes. *Chem. Rev.* **2015**, *115*, 12888–12935.

[32] Hou, W. B.; Hung, W. H.; Pavaskar, P.; Goeppert, A.; Aykol, M.; Cronin, S. B. Photocatalytic conversion of CO_2 to hydrocarbon fuels via plasmon-enhanced absorption and metallic interband transitions. *ACS Catal.* **2011**, *1*, 929–936.

[33] Tu, W. G.; Zhou, Y.; Li, H. J.; Li, P.; Zou, Z. G. Au@TiO_2 yolk-shell hollow spheres for plasmon-induced photocatalytic reduction of CO_2 to solar fuel via a local electromagnetic field. *Nanoscale* **2015**, *7*, 14232–14236.

[34] Robatjazi, H.; Zhao, H. Q.; Swearer, D. F.; Hogan, N. J.; Zhou, L. N.; Alabastri, A.; McClain, M. J.; Nordlander, P.; Halas, N. J. Plasmon-induced selective carbon dioxide conversion on earth-abundant aluminum-cuprous oxide antenna-reactor nanoparticles. *Nat. Commun.* **2017**, *8*, 27.

[35] Wu, B. H.; Liu, D. Y.; Mubeen, S.; Chuong, T. T.; Moskovits, M.; Stucky, G. D. Anisotropic growth of TiO_2 onto gold nanorods for plasmon-enhanced hydrogen production from water reduction. *J. Am. Chem. Soc.* **2016**, *138*, 1114–1117.

[36] Warren, S. C.; Thimsen, E. Plasmonic solar water splitting. *Energy Environ. Sci.* **2012**, *5*, 5133–5146.

[37] Zhang, P.; Wang, T.; Gong, J. L. Mechanistic understanding of the plasmonic enhancement for solar water splitting. *Adv. Mater.* **2015**, *27*, 5328–5342.

[38] Ueno, K.; Oshikiri, T.; Misawa, H. Plasmon-induced water splitting using metallic-nanoparticle-loaded photocatalysts and photoelectrodes. *ChemPhysChem* **2016**, *17*, 199–215.

[39] Nishijima, Y.; Ueno, K.; Kotake, Y.; Murakoshi, K.; Inoue, H.; Misawa, H. Near-infrared plasmon-assisted water oxidation. *J. Phys. Chem. Lett.* **2012**, *3*, 1248–1252.

[40] Huang, Y. B.; Liu, J.; Cao, D. W.; Liu, Z. M.; Ren, K. K.; Liu, K.; Tang, A. W.; Wang, Z. J.; Li, L.; Qu, S. C. et al. Separation of hot electrons and holes in Au/$LaFeO_3$ to boost the photocatalytic activities both for water reduction and oxidation. *Int. J. Hydrogen Energy* **2019**, *44*, 13242–13252.

[41] Saito, K.; Tanabe, I.; Tatsuma, T. Site-selective plasmonic etching of silver nanocubes. *J. Phys. Chem. Lett.* **2016**, *7*, 4363–4368.

[42] Khanadeev, V. A.; Khlebtsov, N. G.; Burov, A. M.; Khlebtsov, B. N. Tuning of plasmon resonance of gold nanorods by controlled etching. *Colloid J.* **2015**, *77*, 652–660.

[43] Brown, A. M.; Sundararaman, R.; Narang, P.; Goddard III, W. A.; Atwater, H. A. Nonradiative plasmon decay and hot carrier dynamics: Effects of phonons, surfaces, and geometry. *ACS Nano* **2016**, *10*, 957–966.
[44] Govorov, A. O.; Zhang, H.; Gun'ko, Y. K. Theory of photoinjection of hot plasmonic carriers from metal nanostructures into semiconductors and surface molecules. *J. Phys. Chem. C* **2013**, *117*, 16616–16631.
[45] Hou, W.; Cronin, S. B. A review of surface plasmon resonance-enhanced photocatalysis. *Adv. Funct. Mater.* **2013**, *23*, 1612–1619.
[46] Kazuma, E.; Kim, Y. Mechanistic studies of plasmon chemistry on metal catalysts. *Angew. Chem., Int. Ed.* **2019**, *58*, 4800–4808.
[47] Zhang, N.; Han, C.; Fu, X. Z.; Xu, Y. J. Function-oriented engineering of metal-based nanohybrids for photoredox catalysis: Exerting plasmonic effect and beyond. *Chem* **2018**, *4*, 1832–1861.
[48] Shin, H. H.; Koo, J. J.; Lee, K. S.; Kim, Z. H. Chemical reactions driven by plasmon-induced hot carriers. *Appl. Mater. Today* **2019**, *16*, 112–119.
[49] Ma, X. C.; Dai, Y.; Yu, L.; Huang, B. B. Energy transfer in plasmonic photocatalytic composites. *Light Sci. Appl.* **2016**, *5*, e16017.
[50] Zhang, Y. C.; He, S.; Guo, W. X.; Hu, Y.; Huang, J. W.; Mulcahy, J. R.; Wei, W. D. Surface-plasmon-driven hot electron photochemistry. *Chem. Rev.* **2018**, *118*, 2927–2954.
[51] Tatsuma, T.; Nishi, H. Plasmonic hole ejection involved in plasmon-induced charge separation. *Nanoscale Horiz.* **2020**, *5*, 597–606.
[52] Li, X. G.; Xiao, D.; Zhang, Z. Y. Landau damping of quantum plasmons in metal nanostructures. *New J. Phys.* **2013**, *15*, 023011.
[53] Brongersma, M. L.; Halas, N. J.; Nordlander, P. Plasmon-induced hot carrier science and technology. *Nat. Nanotechnol.* **2015**, *10*, 25–34.
[54] Link, S.; El-Sayed, M. A. Size and temperature dependence of the plasmon absorption of colloidal gold nanoparticles. *J. Phys. Chem. B* **1999**, *103*, 4212–4217.
[55] Mock, J. J.; Barbic, M.; Smith, D. R.; Schultz, D. A.; Schultz, S. Shape effects in plasmon resonance of individual colloidal silver nanoparticles. *J. Chem. Phys.* **2002**, *116*, 6755.
[56] Ekinci, Y.; Solak, H. H.; Löffler, J. F. Plasmon resonances of aluminum nanoparticles and nanorods. *J. Appl. Phys.* **2008**, *104*, 083107.
[57] Kelly, K. L.; Coronado, E.; Zhao, L. L.; Schatz, G. C. The optical properties of metal nanoparticles: The influence of size, shape, and dielectric environment. *J. Phys. Chem. B* **2003**, *107*, 668–677.
[58] Lu, G.; Wang, G. L.; Li, H. Effect of nanostructured silicon on surface enhanced Raman scattering. *RSC Adv.* **2018**, *8*, 6629–6633.
[59] Manjavacas, A.; Liu, J. G.; Kulkarni, V.; Nordlander, P. Plasmon-induced hot carriers in metallic nanoparticles. *ACS Nano* **2014**, *8*, 7630–7638.
[60] Dhas, N. A.; Raj, C. P.; Gedanken, A. Synthesis, characterization, and properties of metallic copper nanoparticles. *Chem. Mater.* **1998**, *10*, 1446–1452.
[61] Bernardi, M.; Mustafa, J.; Neaton, J. B.; Louie, S. G. Theory and computation of hot carriers generated by surface plasmon polaritons in noble metals. *Nat. Commun.* **2015**, *6*, 7044.
[62] Sundararaman, R.; Narang, P.; Jermyn, A. S.; Goddard III, W. A.; Atwater, H. A. Theoretical predictions for hot-carrier generation from surface plasmon decay. *Nat. Commun.* **2014**, *5*, 5788.
[63] Zhang, Z. L.; Zhang, C. Y.; Zheng, H. R.; Xu, H. X. Plasmon-driven catalysis on molecules and nanomaterials. *Acc. Chem. Res.* **2019,** *52*, 2506–2515.
[64] Kale, M. J.; Avanesian, T.; Christopher, P. Direct photocatalysis by plasmonic nanostructures. *ACS Catal.* **2014**, *4*, 116–128.
[65] Boerigter, C.; Campana, R.; Morabito, M.; Linic, S. Evidence and implications of direct charge excitation as the dominant mechanism in plasmon-mediated photocatalysis. *Nat. Commun.* **2016**, *7*, 10545.
[66] DuChene, J. S.; Sweeny, B. C.; Johnston-Peck, A. C.; Su, D.; Stach, E. A.; Wei, W. D. Prolonged hot electron dynamics in plasmonic-metal/semiconductor heterostructures with implications for solar photocatalysis. *Angew. Chem., Int. Ed.* **2014**, *53*, 7887–7891.
[67] Hung, S. F.; Xiao, F. X.; Hsu, Y. Y.; Suen, N. T.; Yang, H. B.; Chen, H. M.; Liu, B. Iridium oxide-assisted plasmon-induced hot carriers: Improvement on kinetics and thermodynamics of hot carriers. *Adv. Energy Mater.* **2016**, *6*, 1501339.
[68] Zhang, Z.; Yates, Jr. J. T. Band bending in semiconductors: Chemical and physical consequences at surfaces and interfaces. *Chem. Rev.* **2012**, *112*, 5520–5551.
[69] Sá, J.; Tagliabue, G.; Friedli, P.; Szlachetko, J.; Rittmann-Frank, M. H.; Santomauro, F. G.; Milne, C. J.; Sigg, H. Direct observation of charge separation on Au localized surface plasmons. *Energy Environ. Sci.* **2013**, *6*, 3584–3588.
[70] Lian, Z. C.; Sakamoto, M.; Matsunaga, H.; Vequizo, J. J. M.; Yamakata, A.; Haruta, M.; Kurata, H.; Ota, W.; Sato, T.; Teranishi, T. Near infrared light induced plasmonic hot hole transfer at a nano-heterointerface. *Nat. Commun.* **2018**, *9*, 2314.
[71] Zandi, O.; Agrawal, A.; Shearer, A. B.; Reimnitz, L. C.; Dahlman, C. J.; Staller, C. M.; Milliron, D. J. Impacts of surface depletion on the plasmonic properties of doped semiconductor nanocrystals. *Nat. Mater.* **2018**, *17*, 710–717.
[72] Kriegel, I.; Scotognella, F.; Manna, L. Plasmonic doped semiconductor nanocrystals: Properties, fabrication, applications and perspectives. *Phys. Rep.* **2017**, *674*, 1–52.
[73] Boerigter, C.; Aslam, U.; Linic, S. Mechanism of charge transfer from plasmonic nanostructures to chemically attached materials. *ACS Nano* **2016**, *10*, 6108–6115.
[74] Furube, A.; Du, L. C.; Hara, K.; Katoh, R.; Tachiya, M. Ultrafast plasmon-induced electron transfer from gold nanodots into TiO_2 nanoparticles. *J. Am. Chem. Soc.* **2007**, *129*, 14852–14853.
[75] Ning, Y.; Fielding, L. A.; Nutter, J.; Kulak, A. N.; Meldrum, F. C.; Armes, S. P. Spatially controlled occlusion of polymer-stabilized gold nanoparticles within ZnO. *Angew. Chem., Int. Ed.* **2019**, *58*, 4302–4307.
[76] Wei, R. B.; Kuang, P. Y.; Cheng, H.; Chen, Y. B.; Long, J. Y.; Zhang, M. Y.; Liu, Z. Q. Plasmon-enhanced photoelectrochemical water splitting on gold nanoparticle decorated ZnO/CdS nanotube arrays. *ACS Sustainable Chem. Eng.* **2017**, *5*, 4249–4257.
[77] Zhang, Z. S.; Liu, L. H.; Fang, W. H.; Long, R.; Tokina, M. V.; Prezhdo, O. V. Plasmon-mediated electron injection from Au nanorods into MoS_2: Traditional versus photoexcitation mechanism. *Chem* **2018**, *4*, 1112–1127.
[78] Chai, C.; Liu, J. X.; Wang, Y. W.; Zhang, X. C.; Duan, D. H.; Fan, C. M.; Wang, Y. F. Enhancement in photocatalytic performance of Ag–AgCl decorated with h-WO_3 and mechanism insight. *Appl. Phys. A* **2019**, *125*, 96.
[79] Wang, L.; Lv, D. D.; Yue, Z. J.; Zhu, H.; Wang, L.; Wang, D. F.; Xu, X.; Hao, W. C.; Dou, S. X.; Du, Y. Promoting photoreduction properties via synergetic utilization between plasmonic effect and highly active facet of BiOCl. *Nano Energy* **2019**, *57*, 398–404.
[80] Lu, Z. C.; Zhai, X. T.; Yi, R. H.; Li, Z. Y.; Zhang, R. X.; Wei, Q.; Xing, G. H.; Lu, G.; Huang, W. Photoluminescence emission during photoreduction of graphene oxide sheets as investigated with single-molecule microscopy. *J. Phys. Chem. C* **2020**, *124*, 7914–7921.
[81] Su, L.; Lu, G.; Kenens, B.; Rocha, S.; Fron, E.; Yuan, H. F.; Chen, C.; Van Dorpe, P.; Roeffaers, M. B. J.; Mizuno, H. et al. Visualization of molecular fluorescence point spread functions via remote excitation switching fluorescence microscopy. *Nat. Commun.* **2015**, *6*, 6287.
[82] Chen, T.; Dong, B.; Chen, K. C.; Zhao, F.; Cheng, X. D.; Ma, C. B.; Lee, S.; Zhang, P.; Kang, S. H.; Ha, J. W. et al. Optical super-resolution imaging of surface reactions. *Chem. Rev.* **2017**, *117*, 7510–7537.
[83] Ha, J. W.; Ruberu, T. P. A.; Han, R.; Dong, B.; Vela, J.; Fang, N. Super-resolution mapping of photogenerated electron and hole separation in single metal-semiconductor nanocatalysts. *J. Am. Chem. Soc.* **2014**, *136*, 1398–1408.
[84] Nishi, H.; Sakamoto, M.; Tatsuma, T. Local trapping of energetic holes at gold nanoparticles on TiO_2. *Chem. Commun.* **2018**, *54*, 11741–11744.
[85] Wang, S. Y.; Gao, Y. Y.; Miao, S.; Liu, T. F.; Mu, L. C.; Li, R. G.; Fan, F. T.; Li, C. Positioning the water oxidation reaction sites in plasmonic photocatalysts. *J. Am. Chem. Soc.* **2017**, *139*, 11771–11778.
[86] Bai, S.; Li, X. Y.; Kong, Q.; Long, R.; Wang, C. M.; Jiang, J.; Xiong, Y. J. Toward enhanced photocatalytic oxygen evolution: Synergetic utilization of plasmonic effect and schottky junction via interfacing facet selection. *Adv. Mater.* **2015**, *27*, 3444–3452.

[87] Naldoni, A.; Montini, T.; Malara, F.; Mróz, M. M.; Beltram, A.; Virgili, T.; Boldrini, C. L.; Marelli, M.; Romero-Ocaña, I.; Delgado, J. J. et al. Hot electron collection on brookite nanorods lateral facets for plasmon-enhanced water oxidation. *ACS Catal.* **2017**, *7*, 1270–1278.

[88] Liu, L. Q.; Li, P.; Adisak, B.; Ouyang, S. X.; Umezawa, N.; Ye, J. H.; Kodiyath, R.; Tanabe, T.; Ramesh, G. V.; Ueda, S. et al. Gold photosensitized $SrTiO_3$ for visible-light water oxidation induced by Au interband transitions. *J. Mater. Chem. A* **2014**, *2*, 9875–9882.

[89] Wang, M. M.; Wang, P.; Li, C. P.; Li, H. J.; Jin, Y. D. Boosting electrocatalytic oxygen evolution performance of ultrathin Co/Ni-MOF nanosheets via plasmon-induced hot carriers. *ACS Appl. Mater. Interfaces* **2018**, *10*, 37095–37102.

[90] Silva, C. G.; Juarez, R.; Marino, T.; Molinari, R.; Garcia, H. Influence of excitation wavelength (UV or visible light) on the photocatalytic activity of titania containing gold nanoparticles for the generation of hydrogen or oxygen from water. *J. Am. Chem. Soc.* **2011**, *133*, 595–602.

[91] Wang, L.; Hu, H. Y.; Nguyen, N. T.; Zhang, Y. J.; Schmuki, P.; Bi, Y. P. Plasmon-induced hole-depletion layer on hematite nanoflake photoanodes for highly efficient solar water splitting. *Nano Energy* **2017**, *35*, 171–178.

[92] Kim, J.; Son, H. Y.; Nam, Y. S. Multilayered plasmonic heterostructure of gold and titania nanoparticles for solar fuel production. *Sci. Rep.* **2018**, *8*, 10464.

[93] Zhang, Y. C.; Zhang, Y. L.; Guo, W. X.; Johnston-Peck, A. C.; Hu, Y.; Song, X. N.; Wei, W. D. Modulating multi-hole reaction pathways for photoelectrochemical water oxidation on gold nanocatalysts. *Energy Environ. Sci.* **2020**, *13*, 1501–1508.

[94] DePuccio, D. P.; Landry, C. C. Photocatalytic oxidation of methanol using porous Au/WO_3 and visible light. *Catal. Sci. Technol.* **2016**, *6*, 7512–7520.

[95] Xiong, Y. J.; Zou, L. L.; Pan, Q. G.; Zhou, Y.; Zou, Z. Q.; Yang, H. Photo-electro synergistic catalysis: Can Pd be active for methanol electrooxidation in acidic medium? *Electrochim. Acta* **2018**, *278*, 210–218.

[96] Yang, H.; He, L. Q.; Wang, Z. H.; Lu, X. H.; Li, G. R.; Fang, P. P.; Tong, Y. X. Enhanced photocatalytic activity from mixture-fuel cells by ZnO template-assisted Pd-Pt hollow nanorods. *ChemistrySelect* **2017**, *2*, 9842–9846.

[97] Zhang, P.; Wu, P. Y.; Bao, S. Y.; Wang, Z.; Tian, B. Z.; Zhang, J. L. Synthesis of sandwich-structured AgBr@Ag@TiO_2 composite photocatalyst and study of its photocatalytic performance for the oxidation of benzyl alcohols to benzaldehydes. *Chem. Eng. J.* **2016**, *306*, 1151–1161.

[98] Li, H.; Qin, F.; Yang, Z. P.; Cui, X. M.; Wang, J. F.; Zhang, L. Z. New reaction pathway induced by plasmon for selective benzyl alcohol oxidation on BiOCl possessing oxygen vacancies. *J. Am. Chem. Soc.* **2017**, *139*, 3513–3521.

[99] Boltersdorf, J.; Forcherio, G. T.; McClure, J. P.; Baker, D. R.; Leff, A. C.; Lundgren, C. Visible light-promoted plasmon resonance to induce "Hot" hole transfer and photothermal conversion for catalytic oxidation. *J. Phys. Chem. C* **2018**, *122*, 28934–28948.

[100] Pan, H. Q.; Steiniger, A.; Heagy, M. D.; Chowdhury, S. Efficient production of formic acid by simultaneous photoreduction of bicarbonate and oxidation of glycerol on gold-TiO_2 composite under solar light. *J. CO2 Util.* **2017**, *22*, 117–123.

[101] Sun, Y. R.; Du, C. Y.; Han, G. K.; Wang, Y. J.; Gao, Y. Z.; Yin, G. P.Pt/g-C_3N_4 nanosheet for visible light-induced enhancement of activity for formic acid electro-oxidation. *J. Electrochem.* **2018**, *24*, 262–269.

[102] Tanaka, A.; Hashimoto, K.; Ohtani, B.; Kominami, H. Non-linear photocatalytic reaction induced by visible-light surface-plasmon resonance absorption of gold nanoparticles loaded on titania particles. *Chem. Commun.* **2013**, *49*, 3419–3421.

[103] Tanaka, A.; Ogino, A.; Iwaki, M.; Hashimoto, K.; Ohnuma, A.; Amano, F.; Ohtani, B.; Kominami, H. Gold-titanium(IV) oxide plasmonic photocatalysts prepared by a colloid-photodeposition method: Correlation between physical properties and photocatalytic activities. *Langmuir* **2012**, *28*, 13105–13111.

[104] Yin, Y. Y.; Yang, Y.; Zhang, L. Z.; Li, Y. S.; Li, Z. Y.; Lei, W. W.; Ma, Y. F.; Huang, Z. R. Facile synthesis of Au/Pd nano-dogbones and their plasmon-enhanced visible-to-NIR light photocatalytic performance. *RSC Adv.* **2017**, *7*, 36923–36928.

[105] Yu, H. J.; Miller, C. J.; Ikeda-Ohno, A.; Waite, T. D. Photodegradation of contaminants using Ag@AgCl/rGo assemblages: Possibilities and limitations. *Catal. Today* **2014**, *224*, 122–131.

[106] Xiao, Q.; Connell, T. U.; Cadusch, J. J.; Roberts, A.; Chesman, A. S. R.; Gómez, D. E. Hot-carrier organic synthesis via the near-perfect absorption of light. *ACS Catal.* **2018**, *8*, 10331–10339.

[107] Chen, H. T. Interference theory of metamaterial perfect absorbers. *Opt. Express* **2012**, *20*, 7165–7172.

[108] Ng, C.; Cadusch, J. J.; Dligatch, S.; Roberts, A.; Davis, T. J.; Mulvaney, P.; Gómez, D. E. Hot carrier extraction with plasmonic broadband absorbers. *ACS Nano* **2016**, *10*, 4704–4711.

[109] Zhang, L. C.; Jia, C. C.; He, S. R.; Zhu, Y. T.; Wang, Y. N.; Zhao, Z. H.; Gao, X. C.; Zhang, X. M.; Sang, Y. H.; Zhang, D. J. et al. Hot hole enhanced synergistic catalytic oxidation on Pt-Cu alloy clusters. *Adv. Sci.* **2017**, *4*, 1600448.

[110] DuChene, J. S.; Tagliabue, G.; Welch, A. J.; Cheng, W. H.; Atwater, H. A. Hot hole collection and photoelectrochemical CO_2 reduction with plasmonic Au/P-GaN photocathodes. *Nano Lett.* **2018**, *18*, 2545–2550.

[111] Wang, G. L.; Yi, R. H.; Zhai, X. T.; Bian, R. J.; Gao, Y. Q.; Cai, D. Y.; Liu, J. Q.; Huang, X.; Lu, G. et al. A flexible SERS-active film for studying the effect of non-metallic nanostructures on Raman enhancement. *Nanoscale* **2018**, *10*, 16895–16901.

[112] Lu, G.; Li, H.; Wu, S. X.; Chen, P.; Zhang, H. High-density metallic nanogaps fabricated on solid substrates used for surface enhanced Raman scattering. *Nanoscale* **2012**, *4*, 860–863.

[113] Li, Z. Y.; Huang, X.; Lu, G. Recent developments of flexible and transparent sers substrates. *J. Mater. Chem. C* **2020**, *8*, 3956–3969.

[114] Osawa, M.; Matsuda, N.; Yoshii, K.; Uchida, I. Charge transfer resonance Raman process in surface-enhanced Raman scattering from p-aminothiophenol adsorbed on silver: Herzberg-teller contribution. *J. Phys. Chem.* **1994**, *98*, 12702–12707.

[115] Wu, D. Y.; Liu, X. M.; Huang, Y. F.; Ren, B.; Xu, X.; Tian, Z. Q. Surface catalytic coupling reaction of p-mercaptoaniline linking to silver nanostructures responsible for abnormal sers enhancement: A DFT study. *J. Phys. Chem. C* **2009**, *113*, 18212–18222.

[116] Fang, Y. R.; Li, Y. Z.; Xu, H. X.; Sun, M. T. Ascertaining *p,p*'-dimercaptoazobenzene produced from p-aminothiophenol by selective catalytic coupling reaction on silver nanoparticles. *Langmuir* **2010**, *26*, 7737–7746.

[117] Huang, Y. F.; Zhu, H. P.; Liu, G. K.; Wu, D. Y.; Ren, B.; Tian, Z. Q. When the signal is not from the original molecule to be detected: Chemical transformation of *para*-aminothiophenol on Ag during the SERS measurement. *J. Am. Chem. Soc.* **2010**, *132*, 9244–9246.

[118] Sun, M. T.; Hou, Y. X.; Li, Z. P.; Liu, L. W.; Xu, H. X. Remote excitation polarization-dependent surface photochemical reaction by plasmonic waveguide. *Plasmonics* **2011**, *6*, 681–687.

[119] Canpean, V.; Iosin, M.; Astilean, S. Disentangling sers signals from two molecular species: A new evidence for the production of *p,p*'-dimercaptoazobenzene by catalytic coupling reaction of p-aminothiophenol on metallic nanostructures. *Chem. Phys. Lett.* **2010**, *500*, 277–282.

[120] Huang, Y. Z.; Fang, Y. R.; Yang, Z. L.; Sun, M. T. Can *p,p*'-dimercaptoazobisbenzene be produced from p-aminothiophenol by surface photochemistry reaction in the junctions of a Ag nanoparticle-molecule-Ag (or Au) film? *J. Phys. Chem. C* **2010**, *114*, 18263–18269.

[121] Dong, B.; Fang, Y. R.; Chen, X. W.; Xu, H. X.; Sun, M. T. Substrate-, wavelength-, and time-dependent plasmon-assisted surface catalysis reaction of 4-nitrobenzenethiol dimerizing to *p,p*'-dimercaptoazobenzene on Au, Ag, and Cu films. *Langmuir* **2011**, *27*, 10677–10682.

[122] Zhao, L. B.; Huang, Y. F.; Liu, X. M.; Anema, J. R.; Wu, D. Y.; Ren, B.; Tian, Z. Q. A DFT study on photoinduced surface catalytic coupling reactions on nanostructured silver: Selective formation of azobenzene derivatives from para-substituted nitrobenzene and aniline. *Phys. Chem. Chem. Phys.* **2012**, *14*, 12919–12929.

[123] Zhao, L. B.; Huang, Y. F.; Wu, D. Y.; Ren, B. Surface-enhanced Raman spectroscopy and plasmon-assisted photocatalysis of p-aminothiophenol. *Acta Chim. Sin.* **2014**, *72*, 1125–1138. (in Chinese)

[124] Zhao, L. B.; Zhang, M.; Huang, Y. F.; Williams, C. T.; Wu, D. Y.; Ren, B.; Tian, Z. Q. Theoretical study of plasmon-enhanced surface catalytic coupling reactions of aromatic amines and nitro compounds. *J. Phys. Chem. Lett.* **2014**, *5*, 1259–1266.

[125] Shi, X.; Li, H. W.; Ying, Y. L.; Liu, C.; Zhang, L.; Long, Y. T. *In situ* monitoring of catalytic process variations in a single nanowire by dark-field-assisted surface-enhanced Raman spectroscopy. *Chem. Commun.* **2016**, *52*, 1044–1047.

[126] Peng, T. H.; Miao, J. J.; Gao, Z. S.; Zhang, L. J.; Gao, Y.; Fan, C. H.; Li, D. Reactivating catalytic surface: Insights into the role of hot holes in plasmonic catalysis. *Small* **2018**, *14*, 1703510.

[127] Brus, L. Noble metal nanocrystals: Plasmon electron transfer photochemistry and single-molecule Raman spectroscopy. *Acc. Chem. Res.* **2008**, *41*, 1742–1749.

[128] Thrall, E. S.; Steinberg, A. P.; Wu, X. M.; Brus, L. E. The role of photon energy and semiconductor substrate in the plasmon-mediated photooxidation of citrate by silver nanoparticles. *J. Phys. Chem. C* **2013**, *117*, 26238–26247.

[129] Schlather, A. E.; Manjavacas, A.; Lauchner, A.; Marangoni, V. S.; DeSantis, C. J.; Nordlander, P.; Halas, N. J. Hot hole photo-electrochemistry on Au@SiO_2@Au nanoparticles. *J. Phys. Chem. Lett.* **2017**, *8*, 2060–2067.

[130] Dinesh, V. P.; Biji, P.; Ashok, A.; Dhara, S. K.; Kamruddin, M.; Tyagi, A. K.; Raj, B. Plasmon-mediated, highly enhanced photocatalytic degradation of industrial textile dyes using hybrid ZnO@Ag core-shell nanorods. *RSC Adv.* **2014**, *4*, 58930–58940.

[131] Mondal, S.; De Anda Reyes, M. E.; Pal, U. Plasmon induced enhanced photocatalytic activity of gold loaded hydroxyapatite nanoparticles for methylene blue degradation under visible light. *RSC Adv.* **2017**, *7*, 8633–8645.

[132] He, L. L.; Liu, C. Q.; Tang, J.; Zhou, Y. C.; Yang, H.; Liu, R. Y.; Hu, J. G. Self-catalytic stabilized Ag-Cu nanoparticles with tailored SERS response for plasmonic photocatalysis. *Appl. Surf. Sci.* **2018**, *434*, 265–272.

[133] Lu, G.; Yuan, H. F.; Su, L.; Kenens, B.; Fujita, Y.; Chamtouri, M.; Pszona, M.; Fron, E.; Waluk, J.; Hofkens, J. et al. Plasmon-mediated surface engineering of silver nanowires for surface-enhanced Raman scattering. *J. Phys. Chem. Lett.* **2017**, *8*, 2774–2779.

[134] Al-Zubeidi, A.; Hoener, B. S.; Collins, S. S. E.; Wang, W. X.; Kirchner, S. R.; Jebeli, S. A. H.; Joplin, A.; Chang, W. S.; Link, S.; Landes, C. F. Hot holes assist plasmonic nanoelectrode dissolution. *Nano Lett.* **2019**, *19*, 1301–1306.

[135] Kim, Y.; Smith, J. G.; Jain, P. K. Harvesting multiple electron-hole pairs generated through plasmonic excitation of Au nanoparticles. *Nat. Chem.* **2018**, *10*, 763–769.

[136] Zhao, J.; Nguyen, S. C.; Ye, R.; Ye, B. H.; Weller, H.; Somorjai, G. A.; Alivisatos, A. P.; Toste, F. D. A comparison of photocatalytic activities of gold nanoparticles following plasmonic and interband excitation and a strategy for harnessing interband hot carriers for solution phase photocatalysis. *ACS Cent. Sci.* **2017**, *3*, 482–488.

[137] Xie, W.; Schlücker, S. Hot electron-induced reduction of small molecules on photorecycling metal surfaces. *Nat. Commun.* **2015**, *6*, 7570.